SANDIA REPORT

SAND2007-5890
Unlimited Release
Printed October 2007

The Effects of Composition, Temperature and Sample Size on the Sintering of Chem-Prep High Field Varistors

T. J. Garino and M. A. Rodriguez

Prepared by
Sandia National Laboratories
Albuquerque, New Mexico 87185 and Livermore, California 94550

Sandia is a multiprogram laboratory operated by Sandia Corporation,
a Lockheed Martin Company, for the United States Department of Energy's
National Nuclear Security Administration under Contract DE-AC04-94AL85000.

Issued by Sandia National Laboratories, operated for the United States Department of Energy by Sandia Corporation.

Available to DOE and DOE contractors from
U.S. Department of Energy
Office of Scientific and Technical Information
PO Box 62
Oak Ridge, TN 37831

Telephone: (865) 576-8401
Facsimile: (865) 576-5728
E-Mail: reports@adonis.osti.gov
Online Ordering: http://www.osti.gov/bridge

Available to the public from
U.S. Department of Commerce
National Technical Information Service
5285 Port Royal Rd.
Springfield, VA 22161

Telephone: (800) 553-6847
Facsimile: (703) 605-6900
E-Mail: orders@ntis.fedworld.gov
Online Ordering: http://www.ntis.gov/help/ordermethods.asp?loc=7-4-0#online

SAND2007-5890
Unlimited Release
Printed September 2007

The Effects of Composition, Temperature and Sample Size on the Sintering of Chem-Prep High Field Varistors

Terry J. Garino

Electronic Materials and Nanostructure Materials Department
Sandia National Laboratories
P.O. Box 5800
Albuquerque, NM 87185-1411

Abstract

The sintering behavior of Sandia chem-prep high field varistor materials was studied using techniques including *in situ* shrinkage measurements, optical and scanning electron microscopy and x-ray diffraction. A thorough literature review of phase behavior, sintering and microstructure in Bi_2O_3-ZnO varistor systems is included. The effects of Bi_2O_3 content (from 0.25 to 0.56 mol%) and of sodium doping level (0 to 600 ppm) on the isothermal densification kinetics was determined between 650˚ and 825˚C. At ≥750˚C samples with ≥0.41 mol% Bi_2O_3 have very similar densification kinetics, whereas samples with ≤0.33 mol% begin to densify only after a period of hours at low temperatures. The effect of the sodium content was greatest at ~700˚C for standard 0.56 mol% Bi_2O_3 and was greater in samples with 0.30 mol% Bi_2O_3 than for those with 0.56 mol%. Sintering experiments on samples of differing size and shape found that densification decreases and mass loss increases with increasing surface area to volume ratio. However, these two effects have different causes: the enhancement in densification as samples increase in size appears to be caused by a low oxygen internal atmosphere that develops whereas the mass loss is due to the evaporation of bismuth oxide. In situ XRD experiments showed that the bismuth is initially present as an oxycarbonate that transforms to metastable β-Bi_2O_3 by 400˚C. At ~650˚C, coincident with the onset of densification, the cubic binary phase, $Bi_{38}ZnO_{58}$ forms and remains stable to >800˚C, indicating that a eutectic liquid does not form during normal varistor sintering (~730˚C). Finally, the formation and morphology of bismuth oxide phase regions that form on the varistors' surfaces during slow cooling were studied.

Acknowledgments

The authors would like to thank and acknowledge Steve Lockwood for providing the DOE slugs and the powders used, Dale Zschiesche and Sally Lou for technical support, Bonnie McKenzie for performing the SEM analysis, Ralph Tissot for performing the room temperature XRD analysis, Paul Hlava for performing the microprobe analysis, In addition, we thank Steve Lockwood, Gordon Pike, Bruce Tuttle and Tom Hinklin for helpful discussions and we greatly appreciate the programmatic support from Steve Lockwood, Tim Gardner and Alex Roesler, without which this work could not have been performed. Sandia is a multiprogram laboratory operated by Sandia Corporation, a Lockheed Martin Company, for the United States Department of Energy under contract DE-ACO4-94AL85000.

Table of Contents

List of Figures

List of Tables

1.0 Introduction

A varistor is a highly nonlinear resistor that switches from being highly resistive at low electric fields to being many orders of magnitude more conducting at high electric fields. Varistors are typically used commercially to protect circuits from voltage surges. Although the change from insulating to conducting does not occur at a specific value of the applied electric field, it does happen abruptly enough for the concept of a switching or breakdown field to be useful. This is typically defined as the field where the current density reaches a certain value such as 5 A/cm^2. Commercial varistors have low switching fields, <2 kV/cm. Sandia National Laboratories uses high field varistors in the power supplies for ferroelectric neutron generators. The switching field of these varistors exceeds 40 kV/cm. Above the switching field, the current density (J) of a varistor is related to the applied electric field (E) by:

$$J = KE^{\alpha}$$

where K is a constant and α is the non-linearity coefficient. Generally, α is in the range of 20 to 60, with higher values being more desirable.

Varistors are commonly based on zinc oxide that contains minor amounts of bismuth oxide (~0.5 mol%). A variety of other oxides such as Sb, Pr, Co and Mn may also be present. Varistors are polycrystalline ceramics produced by sintering powders that are usually formed by pressing. The grain boundaries between the ZnO grains develop a potential barrier on the order of several volts with applied external electric field that inhibits current flow at low applied fields. The potential barrier between grains decreases rapidly as the switching field is approached, thus increasing varistor current and providing voltage regulation. Therefore, the grain size of the zinc oxide has a major impact on the switching field. Low field varistors have grains generally >10 μm whereas the grain size of Sandia's chem-prep high field material is <1 μm. This high field varistor material was developed at Sandia in the 1980's.[1,2] In addition to ZnO and Bi_2O_3, it also contains CoO and MnO to increase the non-linearity coefficient, aluminum to inhibit grain growth[3] and thus improve sinterability, and sodium to improve electrical performance.

The present study of the sintering behavior of Sandia chem-prep high field varistor material was performed for several reasons. The first goal of this work was to collect sintering densification data under a variety of conditions of temperature and time for a large number of compositions and other powder synthesis variables. This data can be used to guide future potential

modification in composition and sintering schedule, for example. It can also be helpful, along with the results of other studies, to provide better understanding of the sintering process and the roles of both bismuth oxide and sodium. Next, other factors that effect sintering such as the atmosphere and sample size were investigated since these too can help in understanding the details of the sintering process. Also investigated was the cooling and annealing of these materials after sintering to determine what changes take place and what impact these changes may have on electrical properties. In addition, a thorough literature review was conducted to provide background information to help understand the experimental results.

2.0 Literature Review

2.1 ZnO-Bi_2O_3 Phase Diagram

Since zinc and bismuth oxides are the primary constituents of the Sandia varistor material, the equilibrium phase diagram in this system is important to the understanding of how these materials should behave during thermal processing. Before the binary phase diagram is discussed in detail, the phase behavior of each constituent by itself will be reviewed. Whereas, zinc oxide has only one stable crystalline phase, the hexagonal zincite phase, up to its melting point of 1975˚C, bismuth oxide forms several different crystalline equilibrium and metastable phases.[4,5] The monoclinic α-phase is stable from room temperature up to ~720˚C. Above 720˚C, the structure transforms into a cubic phase which remains the equilibrium structure up to the melting point of 825˚C. Most of the literature sources call this equilibrium high temperature phase the δ-phase. Although many refer to this phase as being face-centered cubic, others[4,6] claim that it is actually simple cubic with a lattice parameter of 5.525Å.

In addition to these two phases, two metastable bismuth oxide phases have been reported. The metastable tetragonal phase, called β-Bi_2O_3, can form either directly from a quenched melt or by cooling the δ-phase.[4,5] The other metastable phase is generally called the γ–phase and has a body-centered cubic (bcc) structure with a lattice parameter of 10.268Å. This phase is reported as forming during undercooling of δ-Bi_2O_3. Also, it has been reported that β-Bi_2O_3 can be oxygen deficient and that other metastable sub-oxides of bismuth oxide can form.

The phase relations in the ZnO-Bi_2O_3 system have been the subject of several previous investigations that have yielded conflicting results.[7,8] The early work of Levin and Ross[7] indicated that a compound with the stoichiometry of around $7Bi_2O_3$·ZnO and a bcc structure exists in the system. They reported that this compound has a solid solubility range of ~1% and that it melts congruently at ~785˚C. They found a eutectic at ~740˚C between this binary phase and ZnO at ~14 mol% Bi_2O_3. They did not report any solubility of Zn in either the α or the δ–phase of Bi_2O_3. According to Safronov *et al.*[8] the binary bcc compound has the formula $24Bi_2O_3$·ZnO and it melts incongruently at 750˚C. They report that this phase has the sillenite-type structure, identical to γ-Bi_2O_3 but with a slightly smaller lattice parameter of 10.201Å. They report that the eutectic between this phase and ZnO at 740˚C has a composition of 14 mol% ZnO. Other reported stoichiometries for the binary phase include $8Bi_2O_3$·ZnO[9] and $19Bi_2O_3$·ZnO.[10,11] Kosov *et al.*[12] reported the existence of two binary compounds, $9Bi_2O_3$·ZnO, which melts incongruently at 747˚C and $6Bi_2O_3$·ZnO, which melts congruently at 755˚C. They claim that $9Bi_2O_3$·ZnO phase transforms to the cubic sillenite structure at 737˚C during cooling.

A more recent and complete phase diagram of the ZnO-Bi_2O_3 system has been produced by Guha *et al*.[13] They claim that the binary compound is $19Bi_2O_3$·ZnO (or at 5 mol% ZnO), in agreement with Craig *et al*[10]. and Radaev *et al.*[11], and that it melts incongruently at 753˚C, similar to Safronov *et al*.[8] However, contrary to other sources, they claim that the equilibrium high temperature phase of bismuth oxide is the γ-phase instead of the δ-phase. Their phase diagram is shown in Figure 1. They show the binary phase as a line compound with no solid solubility of either ZnO or Bi_2O_3. The x-ray diffraction patterns of samples with compositions between the binary compound and 2.2 mol% ZnO (the maximum solid solubility they found for ZnO in γ-Bi_2O_3) quenched from 730˚C show that both the binary phase and the γ-Bi_2O_3 phase are present. The similarity between the crystal structures of these two phases has most likely contributed to some of the confusion in the literature where the binary phase may have been misidentified as γ-Bi_2O_3. The eutectic in their diagram between the binary phase and ZnO occurs at a temperature of 738˚C and at a composition of 25 mol% ZnO. This phase diagram predicts that in a simple varistor containing ~0.5 mol% bismuth oxide with the balance being ZnO, no liquid should form until 738˚C and if thermodynamic equilibrium is maintained, the final phase assemblage should contain only ZnO and the binary $19Bi_2O_3$·ZnO phase, regardless of the sintering temperature.

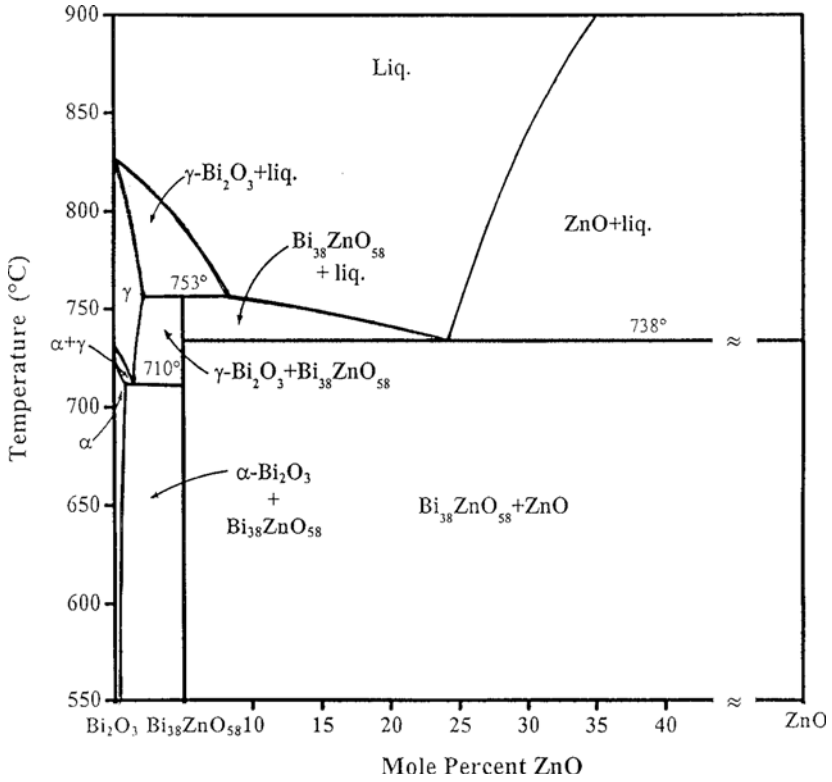

Figure 1. The ZnO – Bi_2O_3 phase diagram of Guha *et al*.[13]

Although most of the published phase diagrams of the ZnO-Bi_2O_3 system do not indicate any solubility of bismuth in ZnO and none was found in some analytical studies[14] there has been some evidence to the contrary. In unpublished work performed at M.I.T. by T. Maruyama in 1978 (referenced in the Master's Thesis of E. Rothman[15]) found the solubility of Bi_2O_3 in ZnO to be 0.17 mol% at the eutectic temperature. More recently, Hwang *et al*[16]. concluded that the solubility of Bi_2O_3 in ZnO at the eutectic temperature is 0.24 ± 0.04 mol%, using analytical electron microscopy (AEM), electron probe microanalysis (EPMA), and secondary ion mass spectrometry (SIMS). They determined that the solubility decreases rapidly with increasing temperature above the eutectic. This may explain why some researchers have failed to find any Bi present in ZnO since material quenched from high temperature would have an amount below the detectability limit of most analytical techniques.

Phase analyses of varistor samples by x-ray diffraction and TEM have found a variety of bismuth oxide phases. The β-phase has been found to exist is some varistor compositions by Takemura *et al.*[17] who found that this phase transformed to the γ–phase with annealing at 600˚C. They state

that this phase transformation negatively impacts the electrical properties of the varistor and they suggest that this is due to the stress caused by the thermal expansion mismatch between the ZnO and the bismuth oxide phase. The stress affects the potential barrier at the grain boundaries and thus the electrical properties of the varistor. A similar result of the β-phase transforming to the γ–phase was found by Cerva and Russwurm[18] whereas Kim *et al.*[19] found that as-sintered samples contained the α-phase which transformed to the γ–phase with annealing at 750˚C. These authors make no mention of a binary phase but it is possible that what they refer to as the γ–phase is actually the binary phase. Interestingly, Cerva and Russwurm[18] did find evidence of Zn in the bismuth oxide phases using STEM microanalysis, although they attribute the Zn signal to the surrounding ZnO matrix due to scattering from the heavy Bi atoms. On the other hand, Olsson *et al*[20]. found both α and δ-Bi_2O_3 in antimony-containing varistor samples sintered at 1200˚C, regardless of the sintering time or the cooling rates. In another study, Olsson *et al.*,[21] quenched similar antimony-containing varistor samples from various temperatures after sintering and found that only δ-Bi_2O_3 was present in samples quenched from 800˚C or above, whereas the γ–phase was the only phase detected after quenching from 600˚, 400˚ or 200˚C. Interestingly, when samples that had been quenched from the sintering temperature were reheated and annealed for one hour before quenching, the γ–phase was present by itself when the anneal temperature was 630˚ or 730˚C. Both phases were present after a 520˚C anneal whereas only the δ-phase was present after the other anneals (230˚, 320˚, 420˚, 840˚ and 940˚C). From their paper it seems that what they call the γ–phase is actually the binary compound. Others have also found that the γ–phase (more likely the binary phase) forms in varistors annealed between 600˚ and 800˚C.[22,23] Finally, using high-temperature x-ray diffraction on the Sandia chem-prep material (non-Na-doped), Rahaman *et al*[24]. claim that at 600˚C an unspecified crystalline Bi_2O_3 phase is present but that by 700˚C, the crystalline Bi_2O_3 no longer remains.

The phase relationships and behavior of the chem-prep high field varistor material is further complicated by the presence of the other dopants, cobalt, manganese and sodium. Of these, sodium is thought to have the largest impact even though it is only present at a concentration of several hundred ppm (typically ~300 ppm). This is because of the effectiveness of sodium oxide as a flux. Previous studies by Hammetter and Voigt[25] using differential thermal analysis indicated that the eutectic temperature in the Na_2O-Bi_2O_3 binary could be ~683˚C.

2.2 Sintering Behavior in the $ZnO\text{-}Bi_2O_3$ Varistor System

The sintering behavior of zinc oxide-based varistor materials containing bismuth oxide has been studied by many researchers. However, most of these studies focus on the sintering behavior at high temperatures, well above the reported eutectic temperature in the $ZnO\text{-}Bi_2O_3$ system since commercial low-field varistors are typically sintered at temperatures above 1000˚C. A liquid phase is clearly present during sintering in this temperature regime so that liquid-phase sintering occurs. Sandia chem-prep high-field varistor material has been sintered typically at temperatures below the binary eutectic, in the range of 710˚ to 740˚C. Therefore only studies on low temperature sintering, including those done on the Sandia material, will be reviewed here.

Two primary effects of bismuth oxide on the low temperature sintering of zinc oxide have been firmly established. First, at low doping levels, from as low as 0.01 to ~0.3 mol%, bismuth oxide impedes the sintering of zinc oxide. In other words, in this regime, pure ZnO will sinter to a higher density at a given temperature than the same ZnO powder doped with bismuth oxide. Second, at higher concentrations, bismuth oxide enhances the sintering of zinc oxide at temperatures below the binary eutectic temperature. Although there is agreement as to the existence of these effects, there is disagreement as to the cause of each.

Both of these effects were noted by Kim *et al*[26]., who studied the sintering behavior in the $ZnO\text{-}Bi_2O_3$ system without any other additives, as a function of bismuth oxide content (0, 0.01, 0.1, 0.5, 2.0 and 5.0 mol%) and temperature. They found that, compared to the undoped ZnO powder, samples with 0.01 and 0.1 mol% Bi_2O_3 displayed significantly impeded densification behavior, whereas the higher bismuth oxide levels enhanced the sintering behavior. The behavior at the low bismuth oxide levels will be discussed first. During heating at 5˚C/min, the undoped powder began shrinking just above 600˚C during heating at 5˚C/min and reached 10% linear shrinkage at ~800˚C. The powder with 0.01 mol% bismuth oxide did not begin to shrink until above 800˚C and did not reach 10% shrinkage until ~950˚C. The 0.1 mol% powder also began to shrink around 800˚C but then shrank rapidly to 10% at 900˚C. Whether the bismuth oxide was added as a powder or as colloidal bismuth hydroxide with 0.09 μm particles had little effect on this behavior. Gardner *et al*[27]. reported that Sandia chem.-prep high-field varistor material behaved similarly. During isothermal sintering at 700˚C, they found that whereas a sample with 0.55

mol% bismuth oxide shrank by nearly 20% in an hour, a sample with 0.415 mol% did not begin to shrink until after 4 hours, at which point it began to shrink at a rate roughly comparable to the initial rate of the 0.55 mol% sample. They also found that a sample with 0.28 mol% bismuth oxide did not shrink at all even after 16 hr at 700˚C.

To explain this behavior, Kim *et al*[26] suggested two possibilities. The first possibility they considered is that bismuth oxide is soluble at low levels in ZnO and once it is in solid solution, it dramatically decreases the solid state sintering kinetics of the ZnO. Although they rule out this possibility because of their own x-ray diffraction results - as well as other published results that do not indicate the presence of Bi in ZnO - others such as Kirkpatrick *et al*[28]. believe this is the correct explanation. They note, as mentioned above, that some studies have indicated that the solubility of bismuth oxide in zinc oxide may be as high as 0.24 mol%. The second explanation proposed by Kim *et al.* is that when the bismuth oxide level is low, the majority of it segregates to the surfaces of the ZnO particles where it impedes neck formation since the presence of the trivalent bismuth ions retards the densification of ZnO. They do not address the fact that this mechanism would apparently also require some solubility of Bi in ZnO. They attribute the onset of significant densification at or above 900˚C in the low Bi_2O_3 samples to the formation of a liquid phase, although they do not explain why that would suddenly occur ~150˚C above the eutectic temperature of ~740˚C. Although it is possible that this could occur as the bismuth oxide comes out of solid solution in the ZnO. However, the formation of a liquid cannot explain the sudden onset of shrinking after 4 hours at 700˚C, well below the eutectic, in the 0.415 mol% bismuth oxide sample of Gardner *et al*.

In a similar manner, two explanations have been put forth to explain the enhanced sintering of ZnO when higher amounts of Bi_2O_3 are present. The first theory is that the enhancement is simply due to liquid phase formation and thus to liquid phase sintering. For example, this is the conclusion of Kim *et al*. even though the enhancement is clear by 700˚C, well below the eutectic temperature. Kirkpatrick *et al*. also favor this theory. Some have suggested that impurities such as sodium in the Sandia chem-prep high-field varistor material may lower the eutectic temperature and thus lead liquid phase sintering below the ZnO-Bi_2O_3 eutectic temperature.

The other explanation for the enhancement in the sub-eutectic sintering of ZnO by bismuth oxide additions greater than ~0.3 mol% is that activated solid state sintering occurs. This was suggested by Rothman[15] who concluded that the presence of bismuth oxide enhanced both the surface and grain boundary diffusion of zinc oxide at temperatures below the eutectic. Gardner *et al*[29]. also concluded that activated sintering occurred for the Sandia material based on their study of the sintering kinetics where significant densification occurs below 700˚C. Rahaman *et al*.[24] and Garino *et al.*[30] also measured appreciable shrinkage starting around 650˚C for the Sandia material. In these cases, the materials that were studied had not been intentionally Na-doped.

More recently, Luo *et al*[31]. have also concluded that a solid-state activated sintering mechanism enhances the densification of ZnO in the presence of sufficient Bi_2O_3. They also found substantial densification in slow heated ZnO powders with 0.58 mol% Bi_2O_3 below 700˚C (compared to the undoped powder which did not measurably shrink). Their TEM analysis revealed Bi segregation to grain boundaries in samples quenched from as low as 650˚C. They found that the grain boundaries of samples heated to 700˚C had an amorphous Bi_2O_3-containing layer ~0.8 μm thick and that a few ZnO particle surfaces also had amorphous Bi_2O_3-containing layer ~1.0 nm thick. These amorphous layers coexisted with crystalline bismuth oxide-rich phase that was found at junctions between ZnO grains. They postulate that this amorphous solid grain boundary film is what provides the high diffusion path in the activated sintering mechanism. To further support this contention, they cite unpublished work that found an increase in oxygen grain boundary diffusion of 10^5-10^6 in samples containing amorphous grain boundary layers as compared to undoped samples.

Other sintering studies on Sandia chem-prep high field varistor materials have found other unusual phenomena that are not fully understood. For example, it was discovered early on in the program that slugs of material sintered to the point where all the remaining porosity was closed had to be thinner than about 1.0 cm or their non-linear coefficient would be below specification.[32] More recently, Lockwood[33] found that the α coefficient met specification in sintered samples without open porosity up to almost 2.5 cm thick. Although this result implies that some type of interaction with the atmosphere, presumably oxygen, is critical, the exact mechanism is unclear. As discussed below, some studies have indicated that excess oxygen at the grain boundaries is necessary for optimum electrical response. However, it is not clear why the

necessary oxygen does not go to the boundaries either prior to the point where the pores close, as it is able to do in samples with residual open porosity, or from the gas trapped in the pores once they close off instead of apparently having to come from the outer surface once the pores have closed. Possibly, the amount of oxygen required is more than is present in the closed pores. Another possibility is that the enhancement of oxygen at the boundaries is only thermodynamically favorable in the temperature regime lower than the sintering temperature so that if oxygen cannot readily reach all the boundaries through an open pore network during cooling, it must come from the outer surface. In either case, annealing a sample after it has been machined into a small rod may allow the needed oxygen to flow in from the surface along the high oxygen conducting grain boundary phase. One other effect that has been noted for Sandia varistor material is that the final sintered density achieved after a specific sintering schedule seems to depend on the size of the varistor sample, with larger samples generally reaching slightly higher density than smaller ones.[34] A similar effect has been noted for standard, high-temperature fired varistors and has been attributed to bismuth oxide volatility.[35,36] However, studies of the mass loss of bismuth oxide indicate that it only becomes appreciable above 1000˚C.[26]

2.3 Grain Boundaries in ZnO-Bi_2O_3 Varistors

Early on in the history of varistors, researchers realized that the grain boundaries were responsible for the highly non-linear electrical behavior by providing a barrier to current flow at low voltage. The thickness of the continuous bismuth-rich grain boundary regions has been the subject of numerous studies.[18,37,38,39,40,41,42] Kobayashi *et al*[43]. used field emission type TEM to show that at relatively thick grain boundaries, ~50 nm, an amorphous bismuth oxide layer ~10 nm thick is sandwiched between two thicker crystalline bismuth oxide layers. At thinner boundaries, ~4 nm thick, the entire layer is amorphous. At other grain boundaries between ZnO grains, they found that only about a half of an atomic layer of Bi was present. Others have also found amorphous bismuth-rich layers in the nm thickness range to be present. In fact Olsson *et al*[44]. measured the breakdown voltage for individual grain boundaries and found it to be 3.6 V when an amorphous layer was present and 3.2 V when only a sub-monolayer of segregated Bi was present. Also, Wang and Chiang[45] have shown that amorphous, nm thick layers can form at

equilibrium below the eutectic temperature and that they have a composition of ~2.3ZnO:1Bi_2O_3, much higher in ZnO than that of the eutectic liquid.

Studies have also established that the distribution of the intergranular bismuth-containing phase is temperature dependent. Work by Gambino, *et al*[46]. indicated, consistent with the suggestion of Baumgartner and Einzinger,[47] that during high temperature sintering (1150˚C), the liquid phase wets to grains with 0˚ contact angle and that the intergranular phase is present at most (88%) of the grain boundaries. When a sample that was cooled slowly from the sintering temperature was examined, they found an average 55˚ dihedral angle and that only 25% of the grain boundaries had the intergranular phase. They also found that when a sample that had been slow cooled from the sintering temperature was annealed at 610˚C and then quenched, no boundaries were found to have the intergranular phase and the dihedral angle was 70˚. This result implies that the intergranular phase is mobile when it is clearly a solid since it receded from the boundaries at 610˚C. Also of interest was the fact that when a sample that had been slow cooled from the sintering temperature was annealed just above the eutectic (780˚C), there was only a slight increase in the percentage of boundaries covered by the intergranular phase (30%) even though the dihedral angle was only 25˚. Presumably, the grain boundaries in these samples that did not have an intergranular phase did have a segregated sub-monolayer of bismuth as has been found by other researchers mentioned above. Subsequent results by Li[48] have shown that the contact angle of the liquid phase on ZnO decreases from about 25˚ at the eutectic temperature to 0˚ at ~920˚C.

Another aspect of the grain boundaries in varistors that has been noted is that an excess of oxygen is present at boundaries with segregated bismuth.[49,50] Stucki and Greuter[48] found that the height of the potential barriers at the grain boundaries depends strongly on the presence of the excess oxygen which can be up to a monolayer. In fact, they even suggest that the primary role that the bismuth plays in the formation of a varistor may be as the means for producing the enrichment in oxygen at the grain boundaries by providing both a network of oxygen conducting pathways and by its segregation that stabilizes the excess oxygen at the boundaries. Several studies have found that annealing varistors in oxygen can be beneficial. For example, Sonder *et al*[51]. found that the electrical properties of varistors that had been heated in reducing atmosphere could be nearly restored by heating at 600˚C in oxygen for 28 hr and that annealing below 540˚C

in oxygen did not improve properties. Ramirez *et al*[52]. were able to restore the varistor behavior in electrically degraded samples by heating at 900˚C in flowing oxygen and that the flow rate of the oxygen was critically important to restoring the high values of α. After annealing at 900˚C in air or oxygen flowing at 5 l/hr, the α was only ~5, even lower than in the degraded sample (17), whereas when the flow rate of oxygen was tripled, the value of α rose to ~52. In one study on Sandia material[30], annealing in oxygen for 0.5 to 2 hr at 700C was found to increase the value of α by 20 to 25%, depending on the prior sintering conditions of the sample.

3.0 Experimental Procedure

For part of this work, slugs of varistor material were used that were made from powder batches that were part of the Design of Experiment (DOE) study carried out by Steve Lockwood and coworkers. For the DOE study, a large number of variables were considered related to powder synthesis, processing and sintering, each one having two possible values. Of these, four were considered to have a possible effect on sintering behavior: Bi_2O_3 content (0.30 or 0.56 mol%), Na doping level (0 or 300 ppm, note that samples not intentionally Na doped had ~100 ppm residual Na from the powder synthesis), the mixing method used during synthesis (standard or shear mixing) and the chloride content that was controlled by the number of times the powder was washed (7 or 10). Table 1 contains a summary of all the materials studied from the DOE samples. They were received as cold isostatically pressed slugs with ~50% green density. A dry diamond saw was used to cut the green slugs into smaller pieces for sintering studies. An isothermal sintering study was performed on samples with 2 hr soaks at temperatures of 720˚, 740˚, 760˚ and 780˚C. Some samples were observed during sintering using a high temperature imaging system in air, argon or oxygen. A tube furnace was used to sinter some of the materials in air or in argon for 2 hr at either 740˚C or 780˚C. Samples from slugs of CPV-78 and 83 were cut into a variety of shapes and sizes to study the effect of this on mass loss and on sintering shrinkage. In this case, a modified “732B” sintering schedule was used that had 2 hr holds at 675˚ and 700˚ before a 16 hr hold at 732˚C. The heating rate differed from the normal B-schedule and was 5˚C/min. Finally, an experiment was performed using three plate-like samples cut from CPV-xx that were sintered together on an alumina plate using the modified 732B schedule. One plate was resting on edge and the other two were resting flat, with one of these covered with an alumina crucible. Again, mass loss and shrinkage were measured.

Table 1. Summary of DOE materials used.

Batch ID	Mixing	Na (ppm)	Bi_2O_3 (mol%)	Cl (# of washes)
CPV-76	Standard	0	0.30	High (7)
CPV-78	Standard	0	0.56	High (7)
CPV-79	Shear	0	0.56	Low (10)
CPV-80	Shear	0	0.30	Low (10)
CPV-82	Shear	300	0.30	High (7)
CPV-83	Standard	300	0.56	Low (10)
CPV-84	Shear	300	0.30	Low (10)
CPV-87	Standard	300	0.30	High (7)
CPV-88	Shear	0	0.56	High (7)
CPV-89	Shear	0	0.30	High (7)
CPV-90	Standard	0	0.56	Low (10)
CPV-92	Standard	300	0.56	Low (10)
CPV-93	Standard	0	0.30	Low (10)

To study a range of compositions of Bi_2O_3 and Na, three powders of different compositions of chem-prep varistor powders received from Steve Lockwood (02454) were mixed together. Powder A was a standard composition powder (0.56 mol% Bi_2O_3, 300 ppm Na) made from several CPV batches. The actual measured Na content of this material was 328 ppm. Powder B was from CPV-121 and was nominally 0.25 mol% Bi_2O_3 and 300 ppm Na (analyzed composition: 0.242 mol% Bi_2O_3, 347 ppm Na). Powders A and B were used by themselves and mixed together in ratios of 1:3, 1:1 and 3:1 to produce intermediate levels of bismuth oxide (powders 2-4 in Table 2). The powders were mixed in deionized water with 1.5 wt% each of dissolved PVA (MW = 15k) and PEG (PEG 20M,). After drying, the mixture was ground with an alumina mortar and pestle and passed through a 150 μm sieve. Powder C, CPV-58, contained the standard amount of bismuth oxide but was not Na-doped (analyzed composition: (0.572 mol% Bi_2O_3, 70 ppm Na). This powder was used by itself and also was mixed with powder A, using the same procedure described above, in ratios of 3:1, 1:1 and 1:3 to give intermediate amounts of Na with essentially the standard amount of bismuth oxide (powders 7-9 in Table 2). A fourth powder, CPV-14C, that had the standard Bi_2O_3 content but was doped with 600 ppm Na

doping was also studied (analyzed composition: 0.555 mol% Bi_2O_3, 660 ppm Na). Pellets were pressed with ~1 g of powder using a 0.5" diameter cylindrical die. The standard pressure used was 15 ksi which gave a green density of ~48% after binder burnout. Some pellets were pressed at other pressures to study the effect of green density on sintering. Samples were heated to 550˚C to remove the binders. Samples were sintered on alumina setter plates in a box furnace with air atmosphere using 5˚C/min heating and the following isothermal hold temperatures: 650˚, 675˚, 700˚, 725˚, 750˚, 775˚, 800˚, 825˚ and 850˚C. At various points during the sintering schedule, the samples were quenched by removing them from the furnace and allowing them to air cool. The diameter of the samples was then measured with calipers and they were then reintroduced to the hot furnace for continued isothermal soaking. After sintering, the final density of the samples was measured using Archimedes technique. The final density and the measured diametral data were than used to determine the density at the various times during the soak.

Table 2. The composition of the powder used for the mixed powder studies.

Powder ID	Nominal Bi_2O_3 (mol%)	Actual Bi_2O_3 (mol%)	Nominal Na (ppm)	Actual Na (ppm)
1	0.56	0.56	300	328
2	0.48	0.481	300	333
3	0.40	0.401	300	338
4	0.32	0.321	300	342
5	0.25	0.242	300	347
6	0.56	0.555	600	660
7	0.56	0.563	225	264
8	0.56	0.566	150	199
9	0.56	0.569	75	135
10	0.56	0.572	0	70

Several other experiments were conducting using the pressed mixed powder samples. Some samples were first sintered at 750˚C for 8 hr and then, once cool, one surface was ground using 600 grit SiC paper. They were then reheated to 750˚C and cooled at 1.5˚C/min while setting on edge. The surfaces of these samples were then examined using optical and scanning electron microscopy (SEM). Elemental analysis was performed on the bismuth oxide containing phase on the surface of one sample using EDS in the SEM. In another experiment, two pellets were first sintered, one with 300 ppm Na and the other without Na doping, at 750˚C for 8 hr. They were

then ground on one surface with 600 grit SiC paper and then each cut into two pieces using a diamond saw. They were then reheated to 750˚C and one half of each pellet was quenched from the furnace while the other half of each was then slow cooled in the furnace at 1.5˚C/min. SEM and x-ray diffraction (XRD) was done on the surfaces of these samples at room temperature. In a separate experiment, images of samples were taken using the high-temperature imaging system of the surfaces of some samples during slow cooling and heating. Finally, *in situ* XRD was performed during heat treating of unsintered and previously sintered materials on both pressed pellets and on thin layers of ground material on top of alumina substrates.

4.0 Results

4.1 DOE Samples

The relative densities of the DOE samples after heating for 2 hr at temperatures from 720˚ to 780˚C are shown in Fig. 2. All the samples with the normal amount (0.56 mol%) of Bi_2O_3 reached a higher density at a given temperature than did any of the samples with the lower level of Bi_2O_3, irrespective of any of the other variables. The densities of the 0.56 mol% Bi_2O_3 samples were all much closer to each other, especially after 740˚C and above than were the 0.30 mol% Bi_2O_3 samples. Also, the for 0.56 mol% Bi_2O_3 samples, there were no clear trends as to how the other variables effected the final density while for the 0.30 mol% Bi_2O_3 samples, the Na-doped samples sintered to higher density than those without additional Na. The main effect of the other variables (mixing type and number of washings) on the densification behavior of the low Bi_2O_3 samples was that those with both standard mixing and 7 washes had a stronger dependence of final density on sintering temperature in that they reached a lower density than otherwise comparable samples at the lowest sintering temperature but reached a higher density than the others at the higher sintering temperatures.

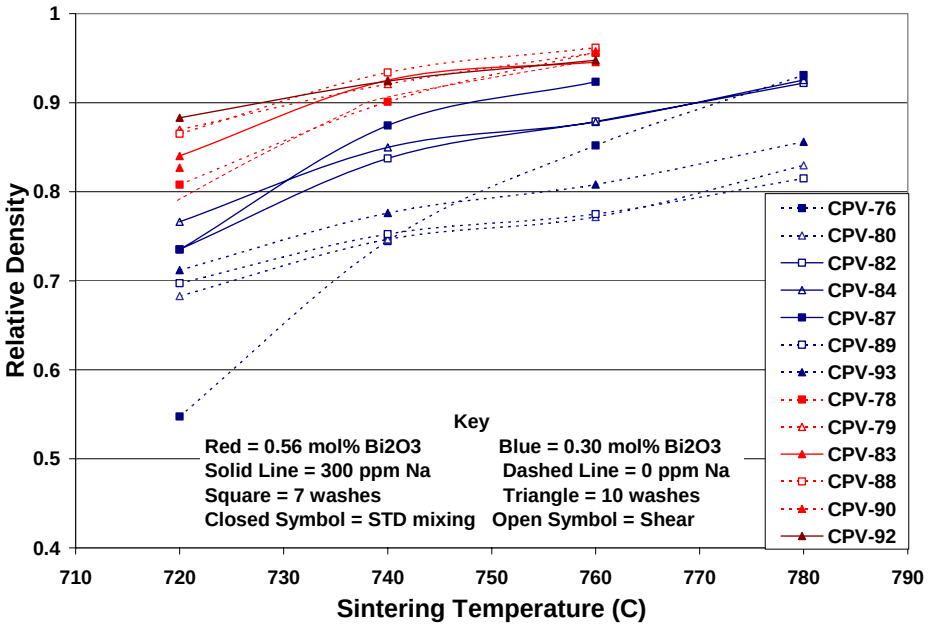

Figure 2. The densification behavior of the DOE samples after 2 hr holds at several temperatures.

The densification behavior during heating at 5˚C/min of 4 of the DOE materials, measured using the *in situ* video system, is shown in Fig. 3. The high Bi_2O_3 samples began to densify just below 700˚C whereas the low Bi_2O_3 samples did not start to densify until around 775˚C. The effect of the Na was most apparent between 850˚ and 900˚C for the low Bi_2O_3 samples, where the Na-doped sample reached a higher density. Comparison of these results with those in Fig. 2 indicate that the low Bi_2O_3 samples have an induction time at sintering temperature below ~800˚C since they reached densities in the 70 to 90% range after holding 2 hr even though they did not densify during heating through that temperature range.

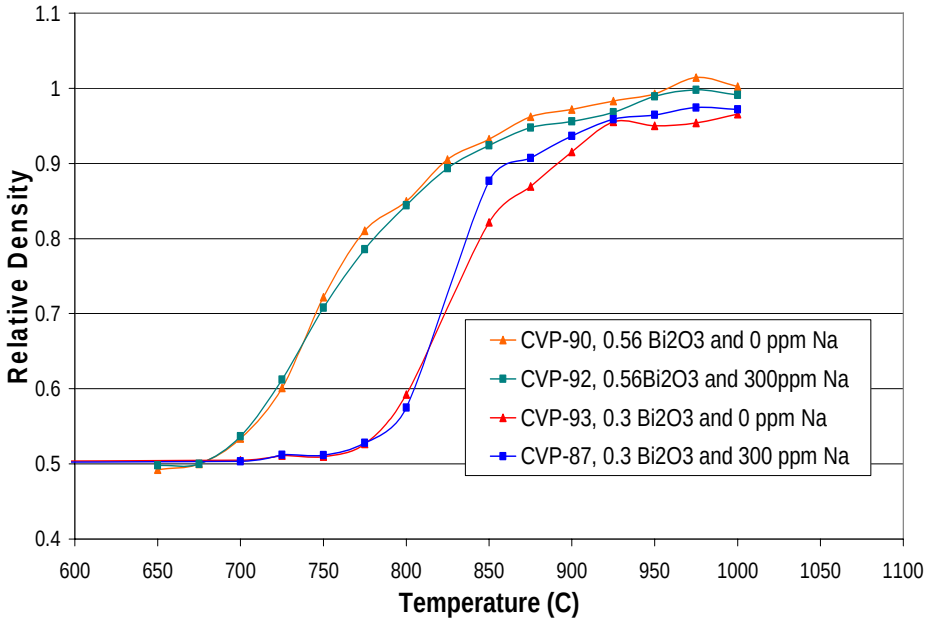

Figure 3. The densification of four DOE samples during heating in air at 5˚C/min measured using the video system.

The densification behaviors of two low Bi2O3 materials are shown during heating in Fig. 4 and during an isothermal hold at 800˚C in Fig. 5 for both oxygen and argon atmospheres. For both materials, densification was enhanced in argon relative to oxygen by roughly a 10% higher relative density. A similar effect was found for a variety of DOE samples that were sintered for 2 hr in both air and argon at either 740˚C (0.56 mol% Bi_2O_3 samples) or 780˚C (0.30 mol% Bi_2O_3 samples), as shown in Fig. 6. For all compositions, samples sintered in argon reached a higher density, in the range of ~2 to ~10%. The increase in density when sintered in argon was generally more for non Na-doped materials.

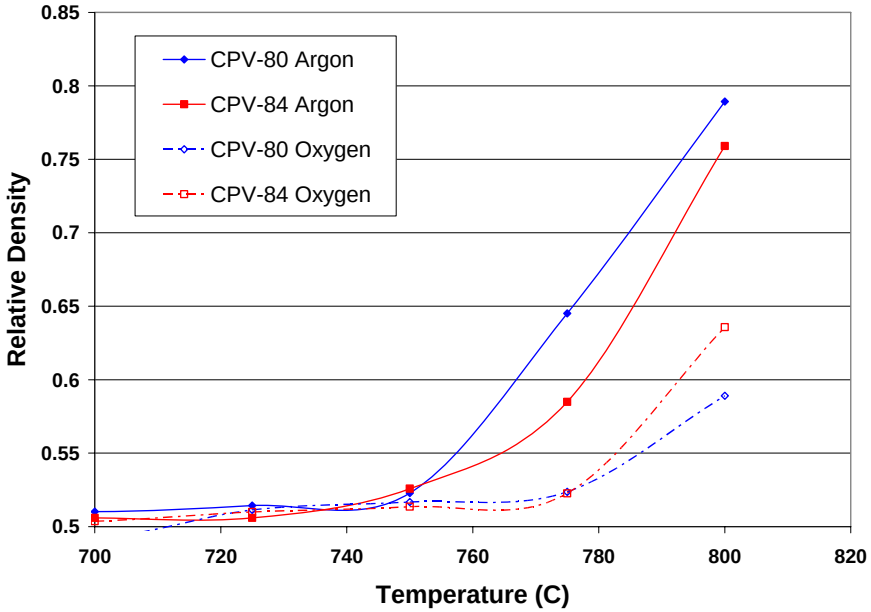

Figure 4. The densification of two low Bi_2O_3 DOE materials during heating at 5˚C/min in both oxygen and argon.

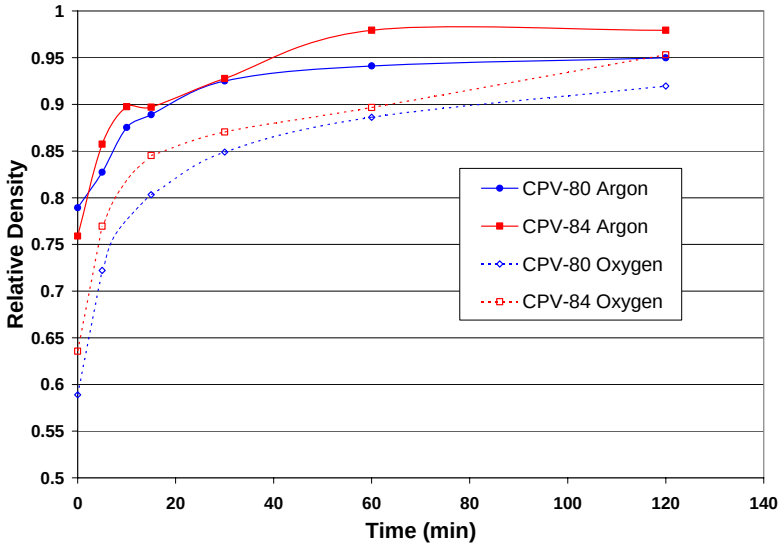

Figure 5. The densification of two low Bi_2O_3 DOE materials during soaking at 800˚C in both oxygen and argon.

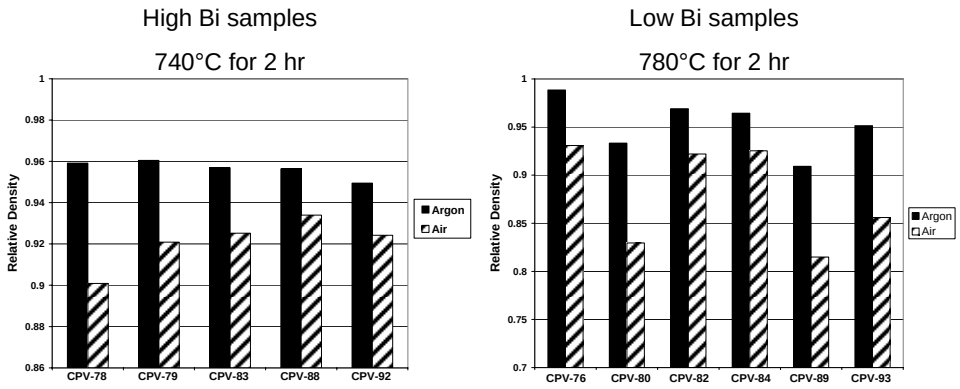

a. b.

Figure 6. Comparison of the sintered densities of DOE samples sintered in either air or argon: a) high Bi_2O_3 samples sintered at 740˚C for 2 hr. and b) low Bi_2O_3 sintered at 780˚C for 2 hr.

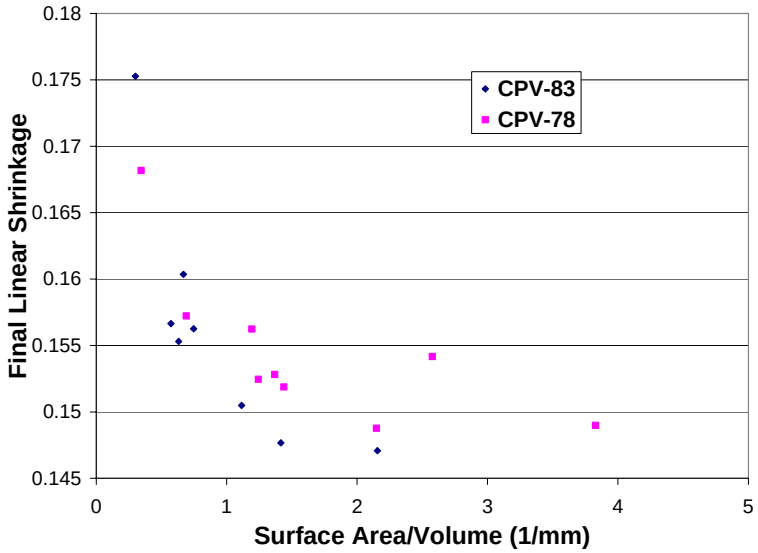

Figure 7. The dependence of final linear shrinkage on surface area to volume ratio for CPV-78 and CPV-83 after sintering for 16 hr at 732˚C (732B schedule).

Fig. 7 shows the final linear shrinkage after sintering in air at 732˚C (using the "B" schedule) of samples from two high Bi_2O_3 DOE materials (CPV-78 and CPV-83) that were a variety of shapes and sizes, plotted against the surface area to volume ratio of the sample. For both materials, there was a decrease in shrinkage of ~2% as the surface area/volume increased. Therefore, larger samples generally sintered to a higher density than smaller ones. A similar trend was seen for CPV- xx samples that were either cubes, plates or rods, as shown in Fig. 8. In this case, the strongest dependence was for the cube-shaped samples whereas there was no dependence for the 3 plate-shaped samples. The mass loss behavior of these same samples is

shown in Figures 9 to 11. Fig. 9 shows how the mass loss changed throughout the sintering schedule for each of the samples. The final mass loss ranged from 0.4% to just over 1% for the samples. Fig. 10 shows that the total mass loss decreased as the size of the sample increased, roughly as the reciprocal of the square root of the minimum linear dimension. Fig. 11 shows that when the same final mass loss data are plotted as a function of the surface area to volume ratio, there is an approximate linear relationship.

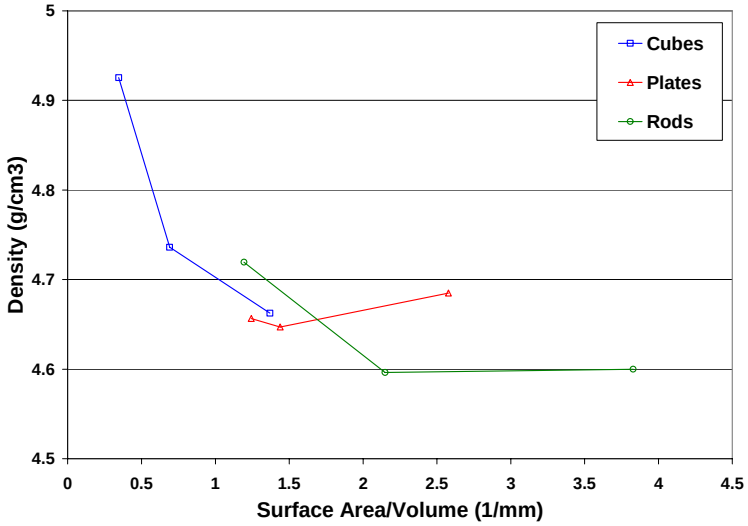

Figure 8. The dependence of final density on surface area to volume ratio for CPV-78 after sintering for 16 hr at 732˚C (732B schedule).

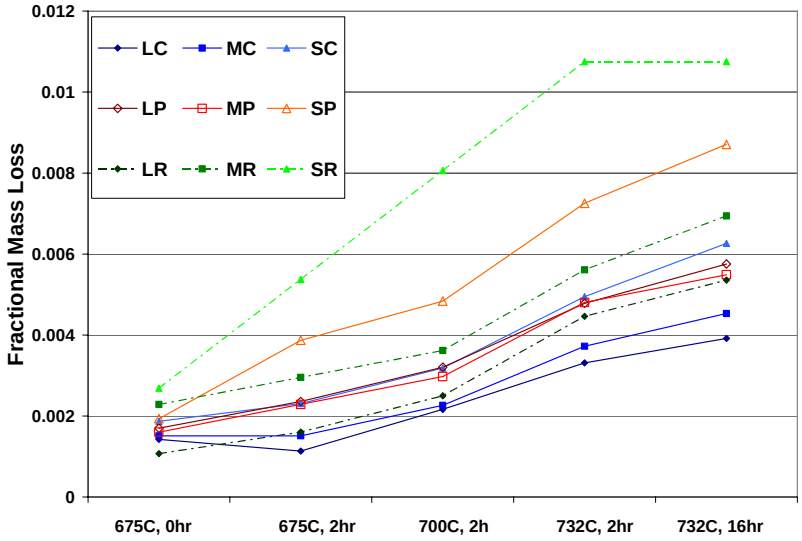

Figure 9. The mass loss of samples CPV-78 of various shapes (C=cube, P=plate and R=rod) and sizes (S=small, M=medium and L=large) at various points in the 732B sintering schedule.

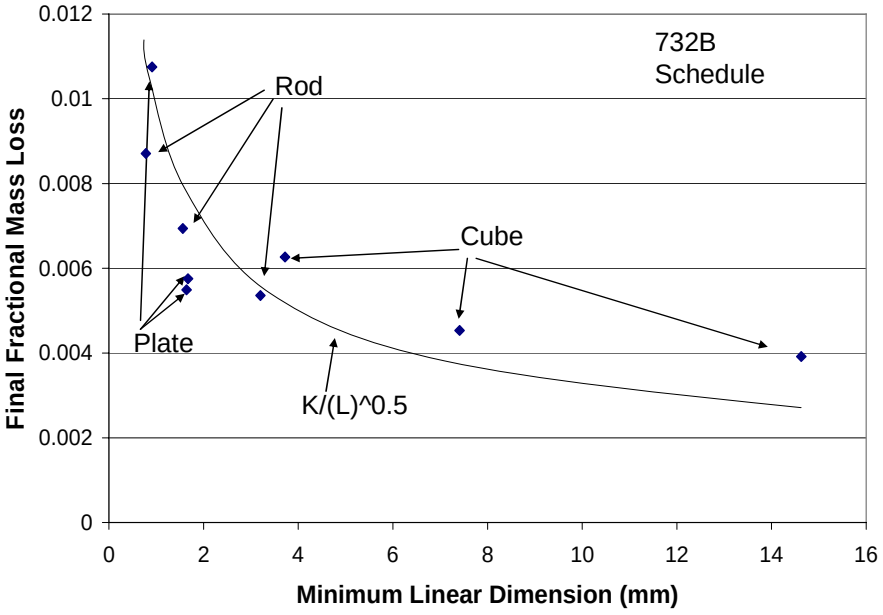

Figure 10. The final mass loss of samples CPV-78 of various shapes and sizes after the 732B sintering schedule as a function of minimum linear dimension.

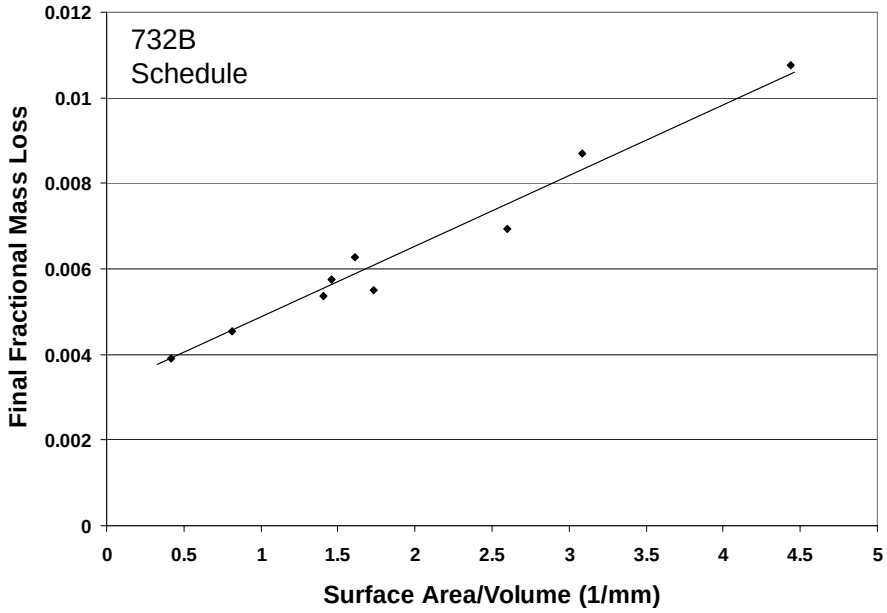

Figure 11. The final mass loss of samples CPV-78 of various shapes and sizes after the 732B sintering schedule as a function of surface area to volume ratio.

The arrangement of three nominally identical, plate-like samples from CPV-78 that were sintered in air using the 732B schedule are shown in Fig. 12. The samples set on an alumina substrate and were each oriented differently. Two were set flat on one of their large surfaces, one of which was covered by an alumina crucible, and the third sample set upright on its smallest edge. The

properties of these samples after 2 and 16 hr at 732˚C are given in Table 2. The upright sample has the highest mass loss and lowest density after each time, and the crucible-covered sample had the lowest mass loss and highest density after the two times. An optical image of an alumina substrate after a sample was sintered lying flat on it is shown in Fig. 13. The inner edge of the dark ring of discoloration corresponds to the location of the edges of the sample. Microprobe analysis indicated the presence of Bi in the discolored region.

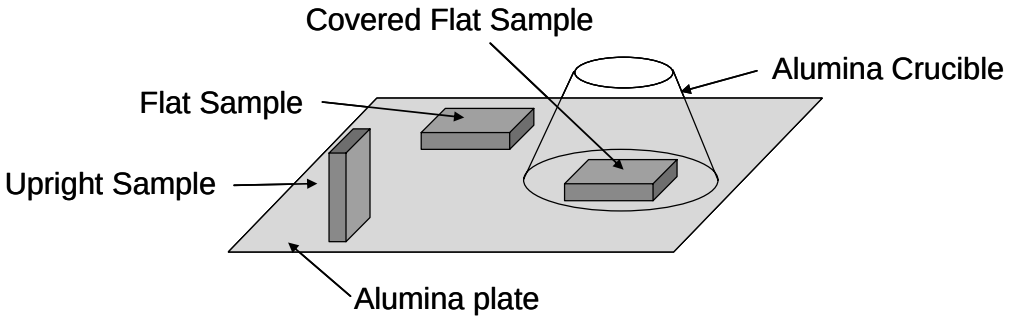

Figure 12. The arrangement of three identical samples of CPV-88 that were sintered using the 732B schedule.

Table 3. The properties of three samples on CPV-88 that were oriented differently during sintering.

	Final Color	Mass Loss 732˚C/2hr	Relative Density 732˚C/2hr	Mass Loss 732˚C/16hr	Relative Density 732˚C/16hr
Upright	Lt. green and white	1.02%	74.3%	0.85%	80.7%
Flat	Med. green	0.71%	77.3%	0.75%	82.9%
Flat and Covered	Dark green	0.68%	82.6%	0.72%	85.0%

Figure 13. Optical micrograph of an initially clean alumina substrate after sintered a CPV-88 sample on it using the 732B schedule.

4.2 Mixed Powder Samples

Figures 14 to 17 and 19 to 22 show the densification behavior of ~1 g varistor pellets with 5 different levels of Bi_2O_3 as a function of time at 650˚, 675˚, 700˚, 725˚, 750˚, 775˚, 800˚ and 825˚C, respectively. All samples had ~300 ppm of Na. At 650˚C (Fig. 14), the samples with the two highest levels of Bi_2O_3 densify to the mid-60% range in the first ~15 hr and then cease further densification over the next 100 hr. The 0.41 mol% sample densified slower, taking ~30 hr to reach its maximum density, but it reached a slightly higher density than did those with the higher Bi_2O_3 levels. The 0.33 mol% sample exhibited only very slight densification after 45 hr but then reached a density comparable to that of the higher Bi_2O_3 samples after another ~67 hr. Since data was not taken between 45 and 112hr, the actual shape of the densification curve in this range is not known. Finally, the sample with the lowest level of Bi_2O_3 did not densify at all even after 112 hr. The data at 675˚C is quite similar (Fig. 15). In this case, the samples with the 4 highest levels of Bi_2O_3 all reach approximately 68% density, with the three highest reaching ~65% after only 8 hr, half the time it took at 650˚C. Once again, it took the 0.41 mol% sample somewhat longer to densify significantly than those with more Bi_2O_3. The 0.33 mol% sample densified a limited amount during the first 8 hr and then it gradually began to densify so that it reached ~64% density after 22 hr and was comparable in density to the higher bismuth oxide samples after 40 hr. After 40 hr, the 0.25 mol% sample had not densified noticeably.

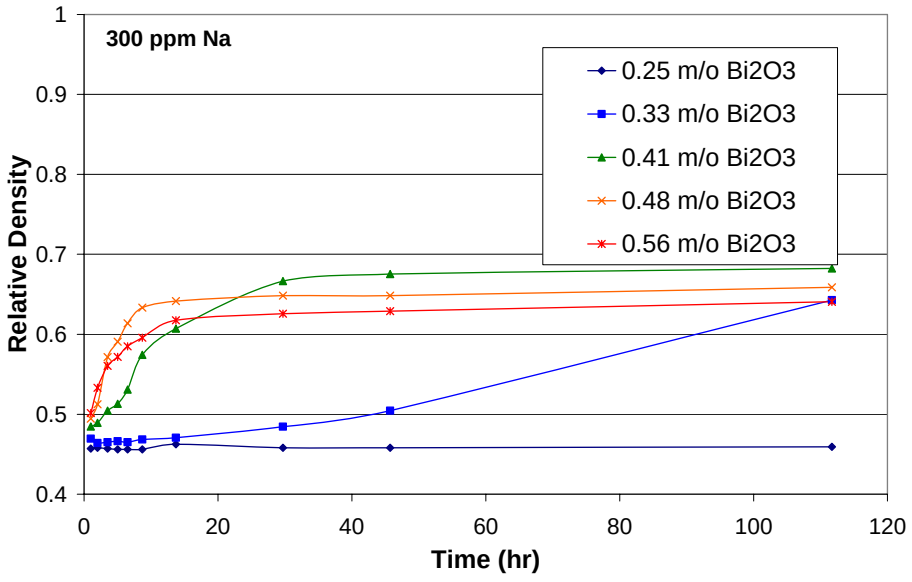

Figure 14. The relative density of varistor samples with various amounts of Bi_2O_3 as a function of time at 650˚C. All samples had 300 ppm Na doping.

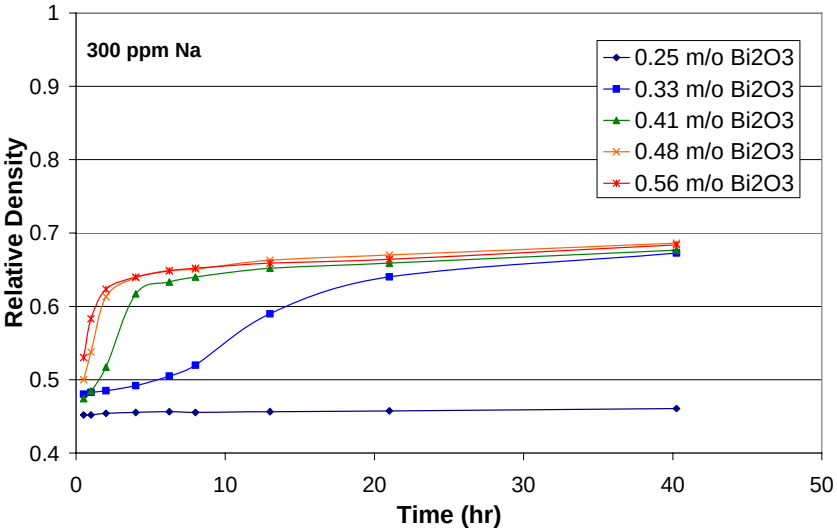

Figure 15. The relative density of varistor samples with various amounts of Bi_2O_3 as a function of time at 675˚C. All samples had 300 ppm Na doping.

At 700˚C (Fig. 16), densification was even more rapid for all samples except the 0.25 mol% Bi_2O_3 one which once again did not undergo significant densification, again after 40 hr. The two samples with the highest Bi_2O_3 levels reached 70% density in ~1 hr, a slightly higher density than they reached after 40 hr at 675˚C. They reached ~80% at 20 hr and ~84% after 40 hr, where it appeared that they were still continuing to densify. Although the densification of the 0.41 and 0.33 mol% samples was still slower than that of the two higher Bi_2O_3 level samples, the differences was less pronounced especially for the 0.33 mol% sample which was only slightly less dense than the others after 10 hr.

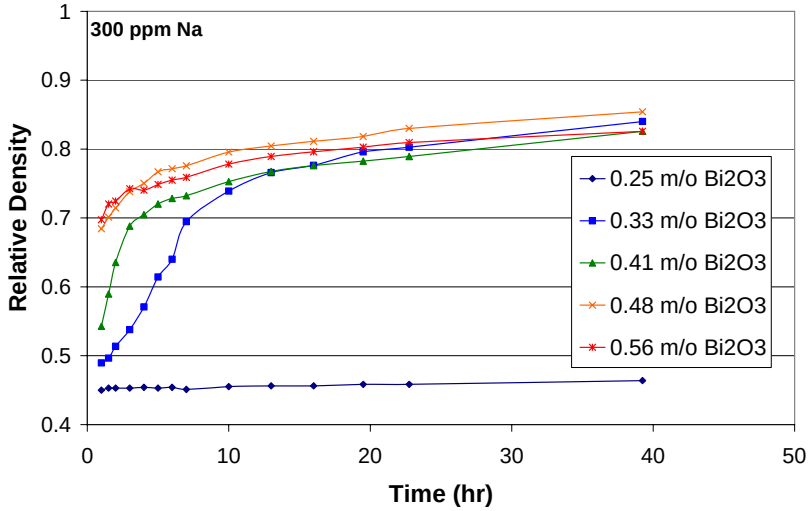

Figure 16. The relative density of varistor samples with various amounts of Bi_2O_3 as a function of time at 700˚C. All samples had 300 ppm Na doping.

Fig. 17 shows that at 725˚C, still below the ZnO-Bi_2O_3 eutectic, the samples with the three highest Bi_2O_3 levels behave quite similarly and reach 90% density after ~16 hr, while the lower level of densification of the 0.33 mol% sample is confined mostly to the first 5 hr. The 0.25 mol% sample did not densify noticeably during the first 16 hr, but reached ~80% density after 33 hr. Fig. 18 shows a composite optical image of a low bismuth oxide sample that has been held at temperature until it begins to densify. This mottled appearance was never observed for high (≥0.41 mol%) Bi_2O_3 samples.

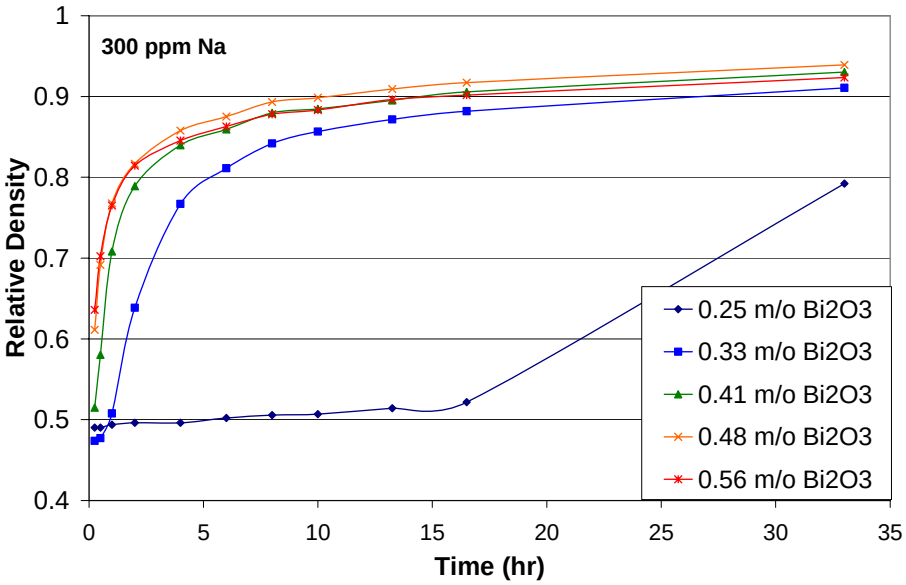

Figure 17. The relative density of varistor samples with various amounts of Bi_2O_3 as a function of time at 725˚C. All samples had 300 ppm Na doping.

Figure 18. A composite optical micrograph of a 0.25 mol% Bi_2O_3 sample after 16 hr at 725˚C.

Fig. 19 shows that at 750˚C, just above the ZnO-Bi_2O_3 eutectic, the samples with the three highest Bi_2O_3 levels again behave quite similarly and now reach ~90% density after ~4 hr. The 0.33 mol% sample is within a few % of the density of the higher Bi_2O_3 samples after ~1.5 hr. At this temperature, the 0.25 mol% sample begins to densify rapidly around 5 hours into the hold and reaches ~90% density after 16 hr, compared to reaching only ~51% after 16 hr at 725˚C.

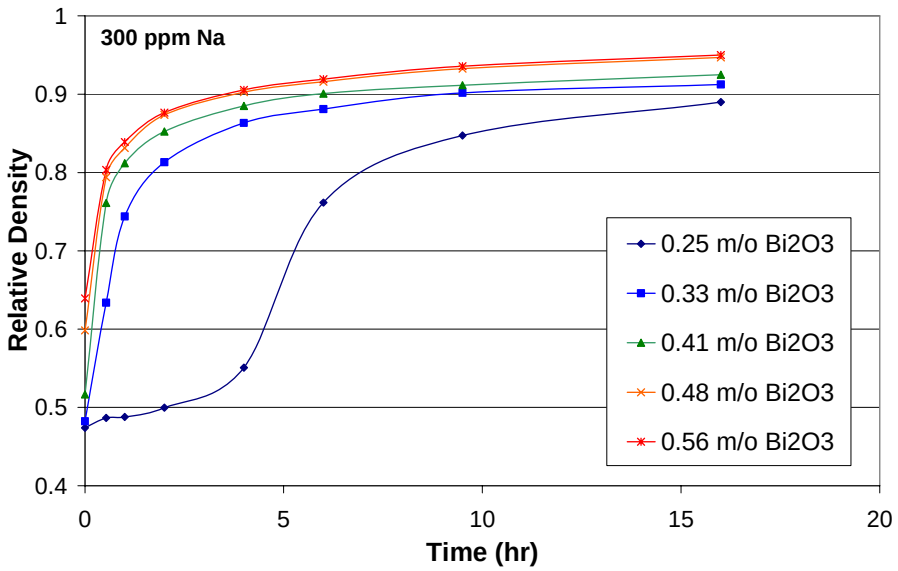

Figure 19. The relative density of varistor samples with various amounts of Bi_2O_3 as a function of time at 750˚C. All samples had 300 ppm Na doping.

The trend towards more rapid densification continues at 775˚C, with all 5 samples reaching ~95% density after only 8 hr (see Fig. 20). The samples with the 4 highest levels of Bi_2O_3 reach ~90% density after only 1 hr, whereas the 0.25 mol% sample begins to densify after ~2 hr and reaches ~90% density after 5 hr. At 800˚C (Fig. 21), only after a 0 hr hold is the 0.33 mol% sample significantly less dense than the higher Bi_2O_3 samples and all 4 reach ~90% density after ~0.5 hr. The 0.25 mol% sample begins to densify after ~0.5 hr and reaches ~90% density after 2 hr.

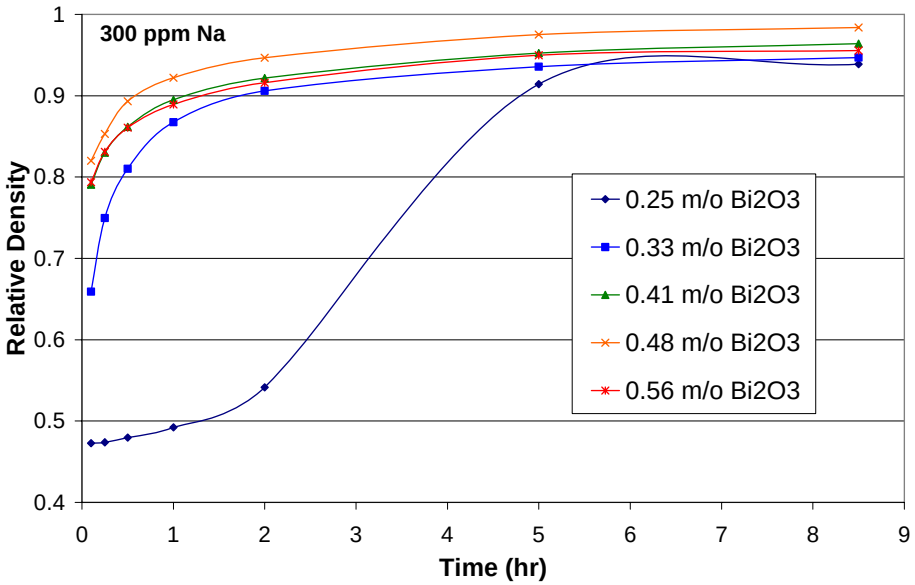

Figure 20. The relative density of varistor samples with various amounts of Bi_2O_3 as a function of time at 775˚C. All samples had 300 ppm Na doping.

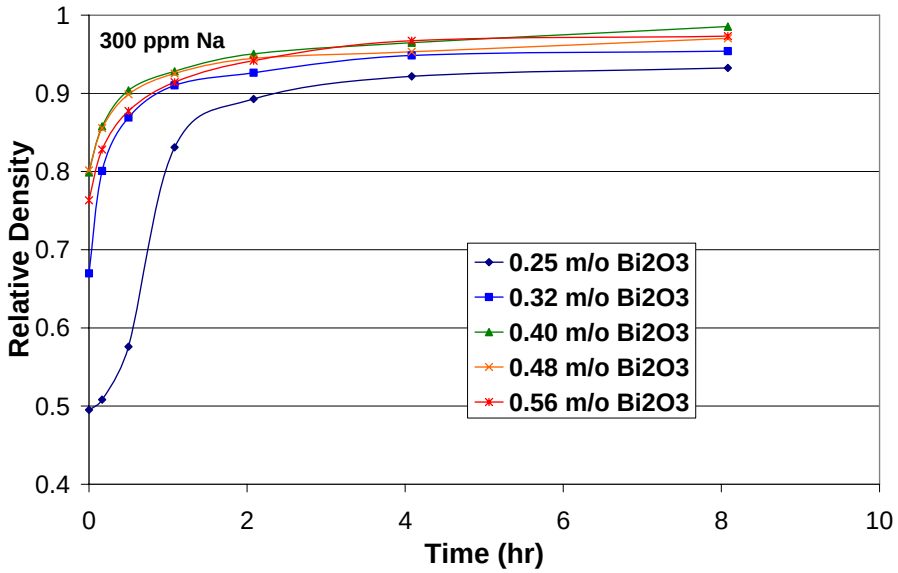

Figure 21. The relative density of varistor samples with various amounts of Bi_2O_3 as a function of time at 800˚C. All samples had 300 ppm Na doping.

Figure 22 shows the results at the highest temperature studied, 825˚C. At this temperature, all samples except the 0.25 mol% one behave nearly identically, reaching 90% density after ~15 min and ~95% after 2 hr. The sample with 0.25 mol% Bi_2O_3 began to densify during the early part of the soak and reached a density of 90% after ~1hr. All the data for the lowest and the

highest bismuth oxide level samples at all temperatures are plotted together for comparison in Figures 23 and 24, respectively.

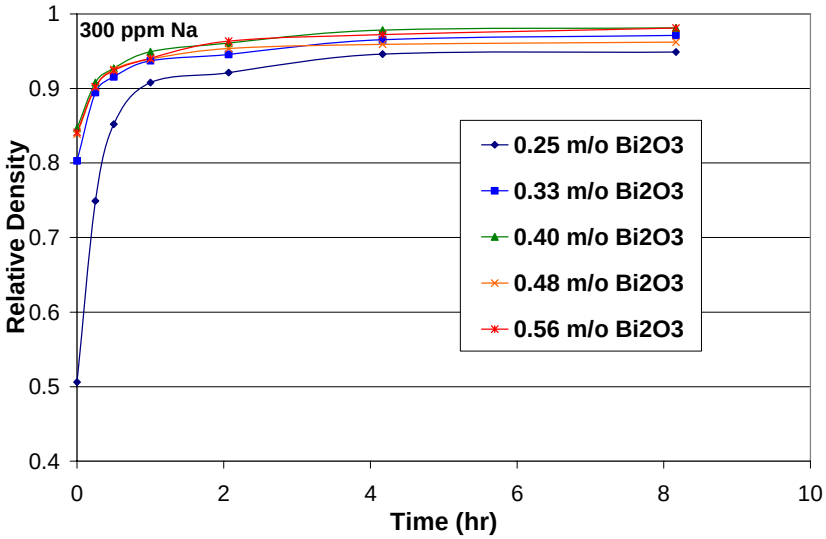

Figure 22. The relative density of varistor samples with various amounts of Bi_2O_3 as a function of time at 825˚C. All samples had 300 ppm Na doping.

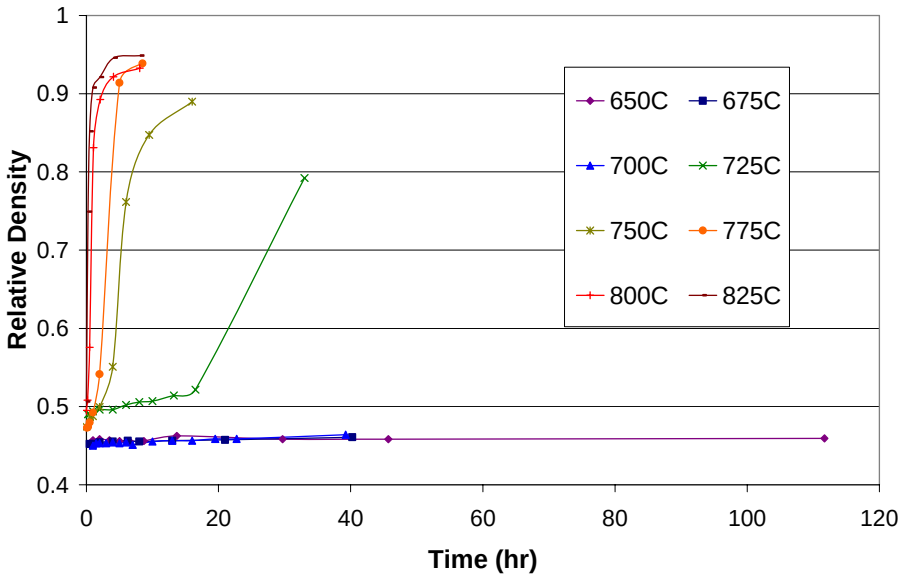

Figure 23. The relative density of varistor samples with 0.25 mol% Bi_2O_3 as a function of time at various temperatures. All samples had 300 ppm Na doping.

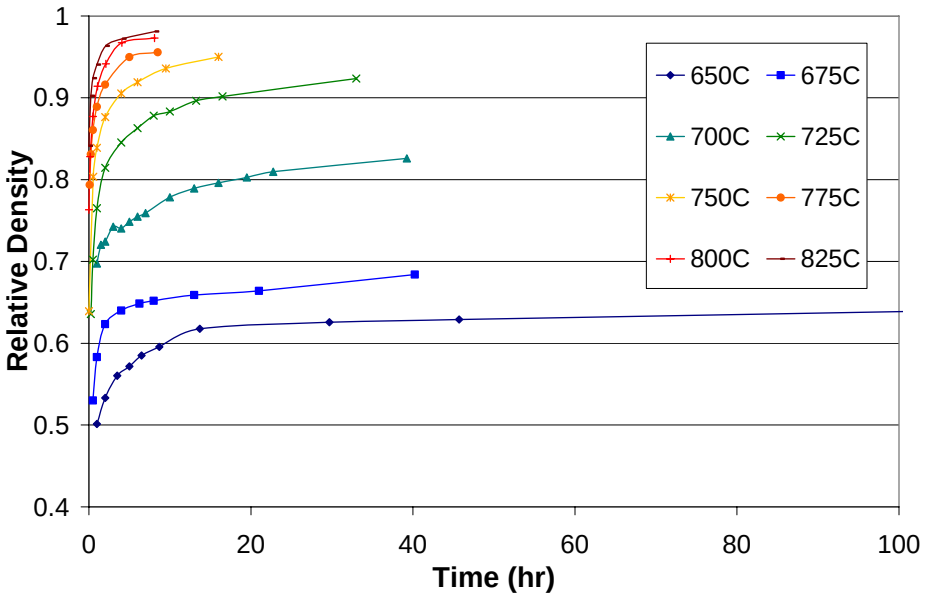

Figure 24. The relative density of varistor samples with 0.56 mol% Bi_2O_3 as a function of time at various temperatures. All samples had 300 ppm Na doping.

The effect of Na concentration on the densification behavior of samples with 0.56 mol% Bi_2O_3 as a function of time at temperatures from 650˚C to 825˚C is shown in Figures 25 to 32. At 650˚C after 40 hr, the samples ranged from ~60% for the 0 and 75 ppm samples to ~65% for the 225 ppm sample (see Fig. 25). Little densification occurred after ~10 hr. The slight differences between the samples may be in part due to slight differences in green density and to measurement error. At 675˚C the final densities after 40 hr ranged from ~65% to just over 70%, with the density increasing with the Na content (see Fig. 26). Once again, little densification occurred after ~10 hr. At 700˚C, Fig. 27, the behavior was significantly different in that there was much more spread in the data for the various amounts of Na. After 16 hr, the 0 ppm sample just reached 70%, the 150 ppm sample 80% and the 600 ppm sample 90%. At 725˚C, Fig. 28, the samples with ≥150 ppm Na all densified similarly, reaching ~90% relative density after ~14 hr. The 75 ppm sample had a relative density that was a few percent less whereas the undoped sample only reached ~78% relative density after the same amount of time. At 750˚C, the spread in densities between the samples became smaller and more uniform, as shown in Fig. 29. The final relative density only ranged from ~91% for the undoped sample to ~95% for the 600 ppm Na sample. The densification behavior was similar to this at the three highest temperatures studied, 775˚C (Fig. 30), 800˚C (Fig. 31) and 825˚C (Fig. 32). The data for all temperatures of plotted together for the undoped sample in Fig. 33 and for the 300 ppm sample in Fig. 34.

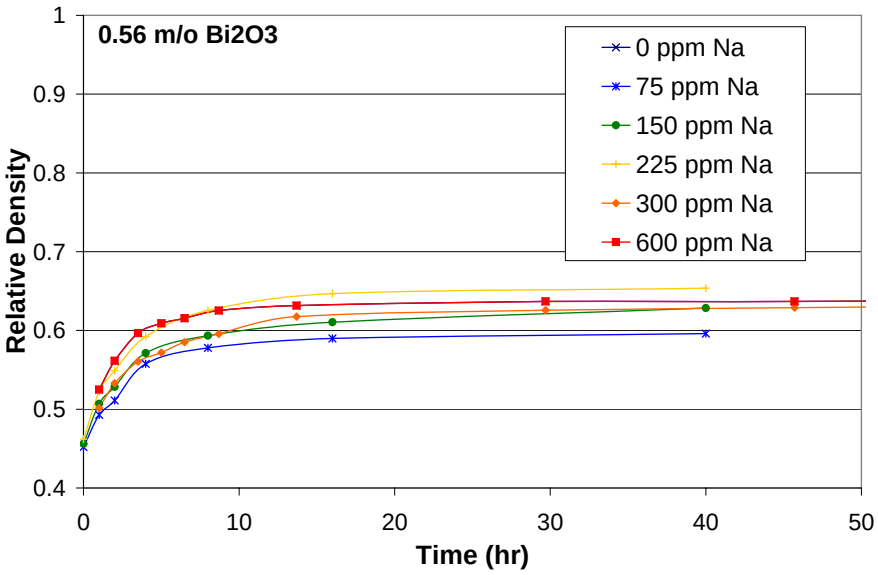

Figure 25. The relative density of varistor samples with 0.56 mol% Bi_2O_3 and various amounts of Na as a function of time at 650˚C.

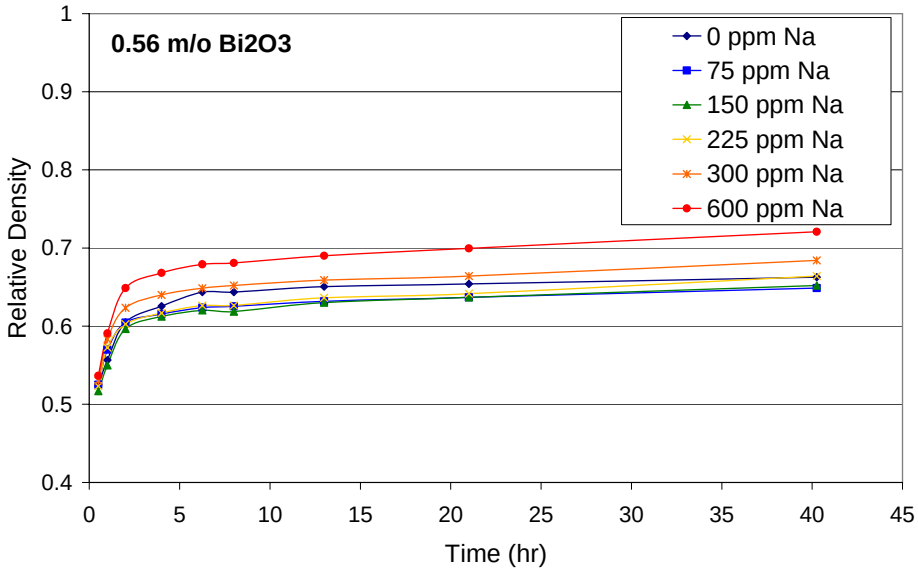

Figure 26. The relative density of varistor samples with 0.56 mol% Bi_2O_3 and various amounts of Na as a function of time at 675˚C.

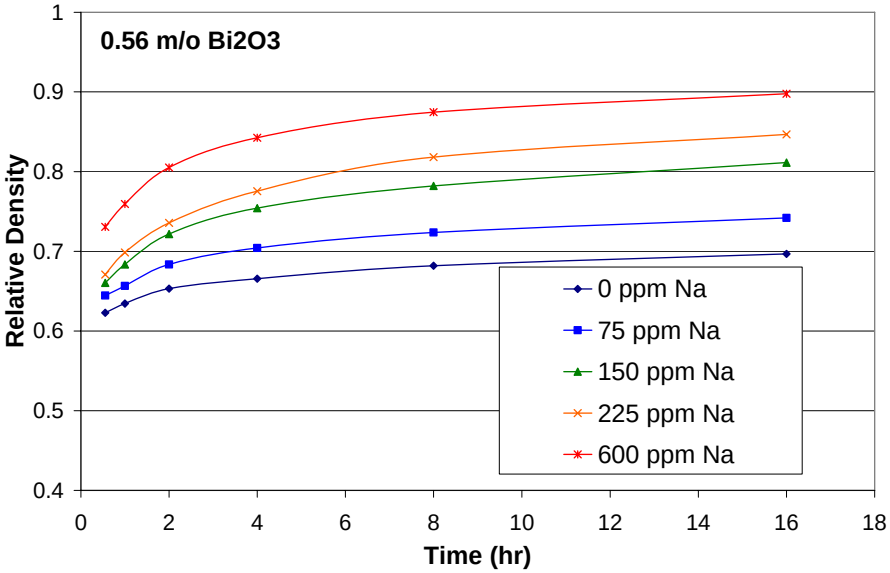

Figure 27. The relative density of varistor samples with 0.56 mol% Bi_2O_3 and various amounts of Na as a function of time at 700˚C.

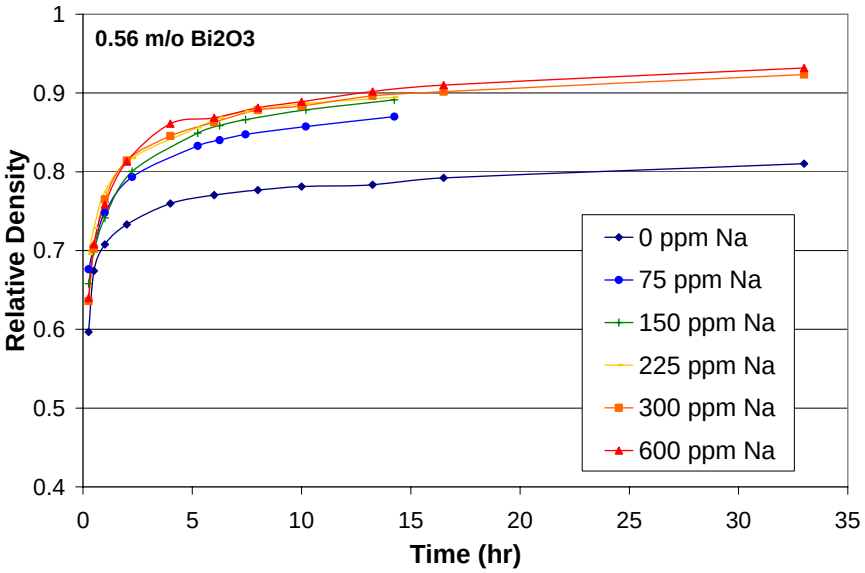

Figure 28. The relative density of varistor samples with 0.56 mol% Bi_2O_3 and various amounts of Na as a function of time at 725˚C.

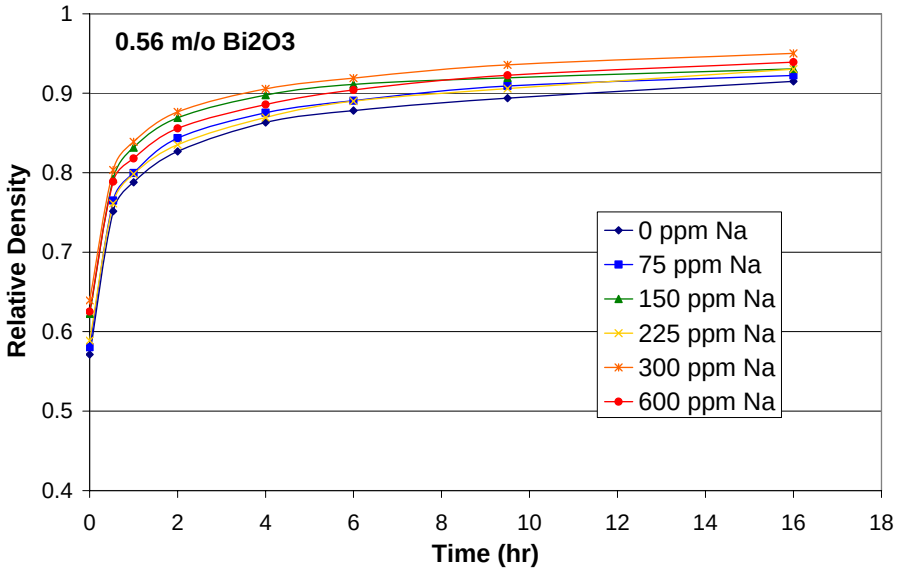

Figure 29. The relative density of varistor samples with 0.56 mol% Bi_2O_3 and various amounts of Na as a function of time at 750˚C.

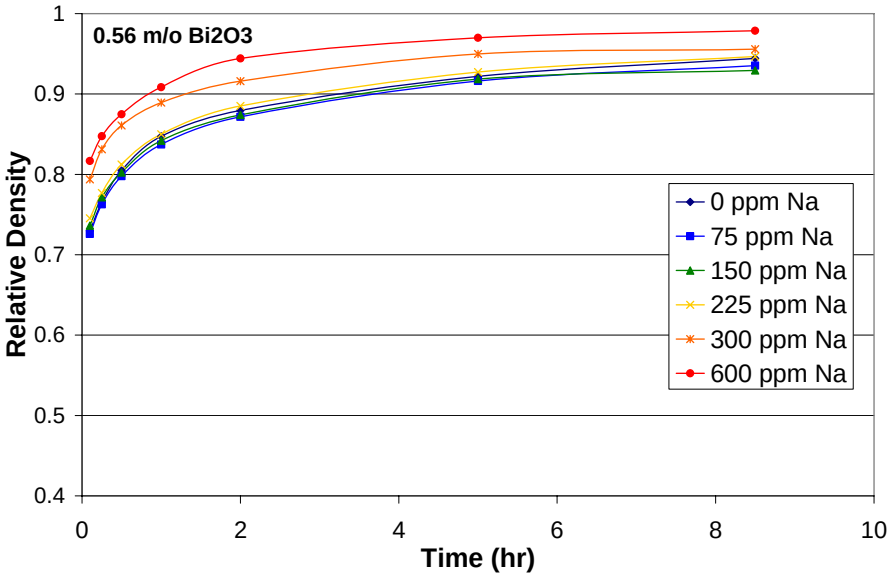

Figure 30. The relative density of varistor samples with 0.56 mol% Bi_2O_3 and various amounts of Na as a function of time at 775˚C.

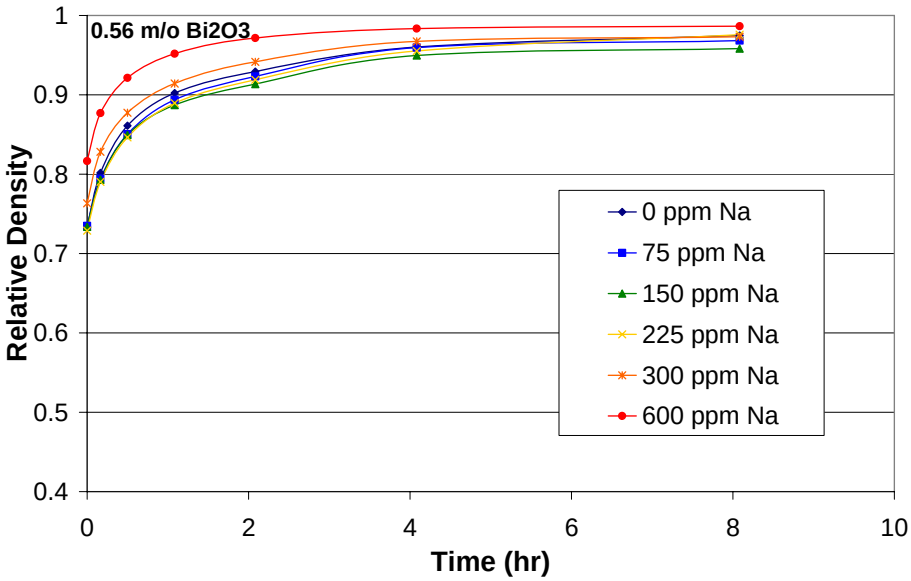

Figure 31. The relative density of varistor samples with 0.56 mol% Bi_2O_3 and various amounts of Na as a function of time at 800˚C.

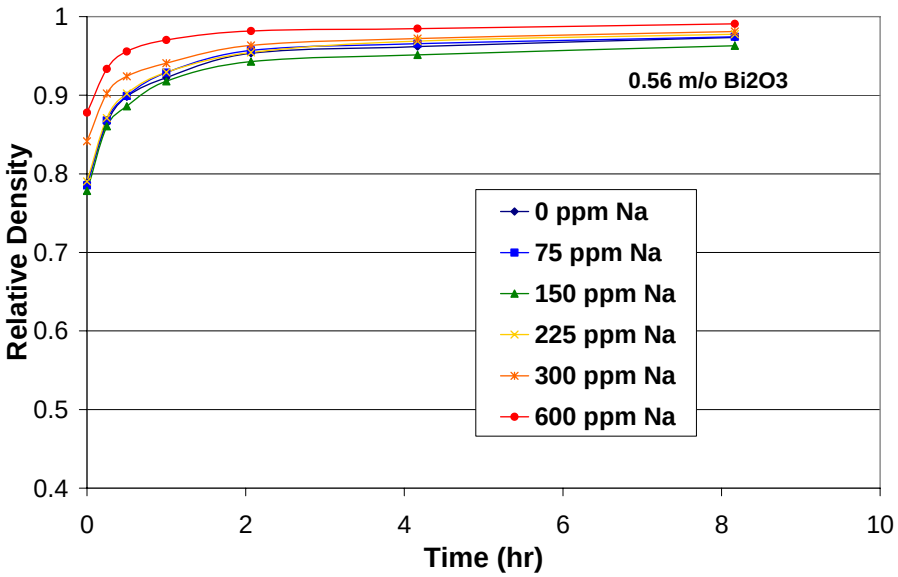

Figure 32. The relative density of varistor samples with 0.56 mol% Bi_2O_3 and various amounts of Na as a function of time at 825˚C.

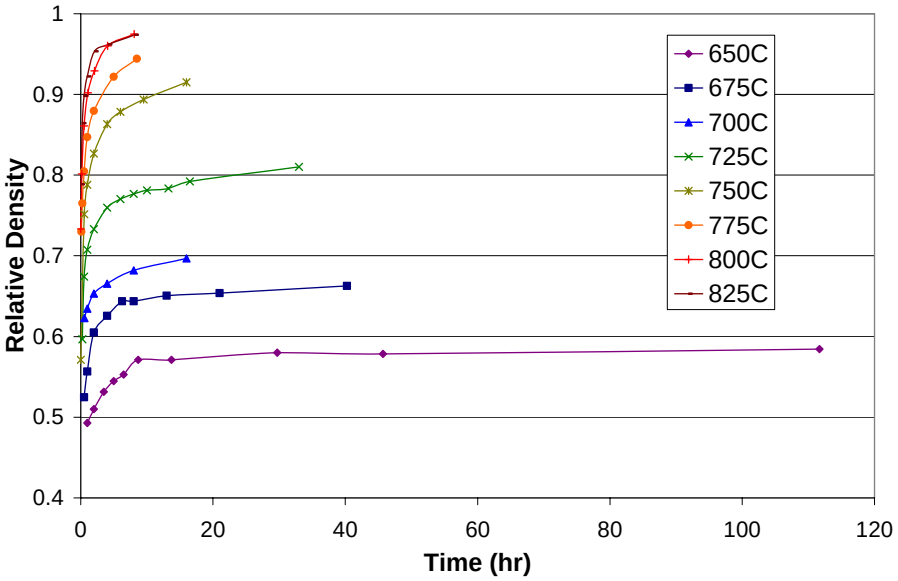

Figure 33. The relative density of varistor samples with no Na doping and 0.56 mol% Bi_2O_3 as a function of time at various temperatures.

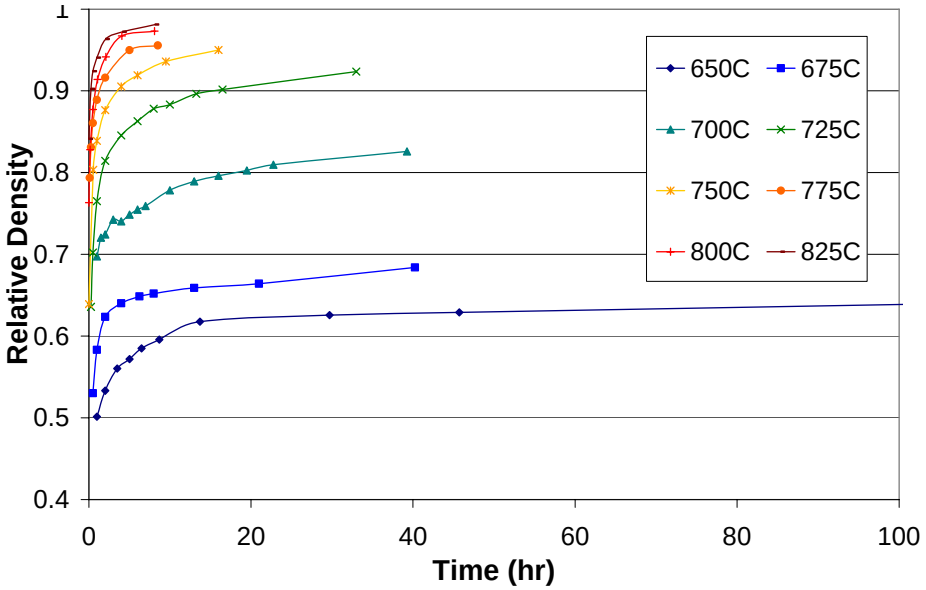

Figure 34. The relative density of varistor samples with 300 ppm Na doping and 0.56 mol% Bi_2O_3 as a function of time at various temperatures.

The effect of green density on the densification behavior of standard composition powder at 725˚C is shown in Fig. 35. Even after 16 hr, the initial differences in density are still very much apparent with the 55% green density sample reaching ~97% relative density, which is about 10% higher than the 40% green density sample.

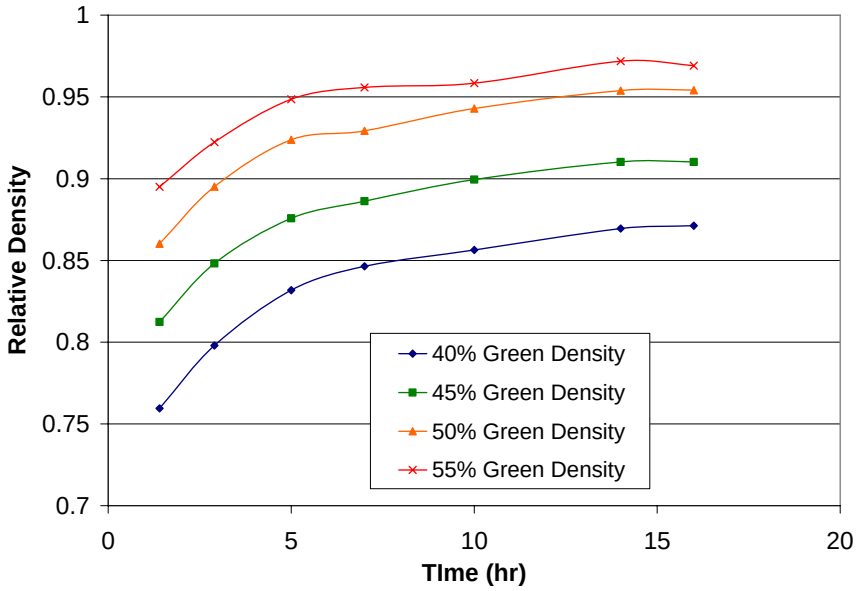

Figure 35. The effect of green density on the densification behavior of standard powder (0.56 mol% Bi_2O_3 and 300 ppm Na) at 725˚C.

Figs. 36 to 43 show optical images of the as-sintered and the as-ground (with 400 grit paper) surface of a variety of varistor samples that had been previously sintered at 725˚C for 16 hr and then cooled, setting on edge, at 1.5˚C/min from 725˚C. These samples differed in Bi_2O_3 content, Na content and green density. The morphology of the Bi_2O_3 phase on the surfaces differs greatly from sample to sample and even between the sintered and the ground surfaces of the same sample. The samples shown in Fig. 36 (0.27 mol% Bi_2O_3, 300 ppm Na and a 55% green density), Fig. 37 (0.29 mol% Bi_2O_3, 300 ppm Na and a 50% green density) and Fig. 38 (0.29 mol% Bi_2O_3, 300 ppm Na and a 55% green density) all had more of the Bi_2O_3 phase near the edge on the as-sintered surface and more on the as-sintered surface than on the ground surface. The sample in Fig. 39 which had a higher Bi_2O_3 content (0.41 mol%) but a lower green density (40%), had a much different appearance with no large regions of the bismuth oxide phase visible. Another sample with 0.41 mol% Bi_2O_3 but with a higher green density of 55% is shown in Fig. 40. In this case there were only a few small regions on the sintered surface whereas the ground surface had a high density of the regions but only near the center of the sample. The sample shown in Fig. 41 had the standard composition and had only a few small regions visible on its surface. However, this result was not typical since, as discussed below, other slow-cooled standard composition samples did have a much higher density of the bismuth oxide phase regions and with a morphology similar to those of the samples in Figs. 36 to 38 (also see Figs 54, 60 to 63). Finally,

the samples without Na doping did not develop any of the large bismuth oxide regions on either surface, with either 50 or 55% green density (see Figs. 42 and 43).

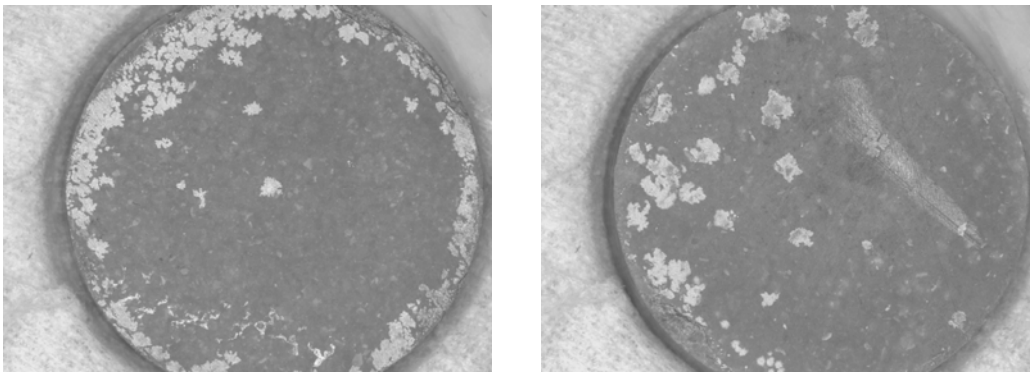

Sintered Surface Ground Surface

Figure 36. Optical micrographs of the as-sintered and the as-ground surfaces of a varistor pellet with 0.27 mol% Bi_2O_3, 300 ppm Na and a 55% green density after sintering at 725˚C for 16 hr in air and then cooling at 1.5˚C/min.

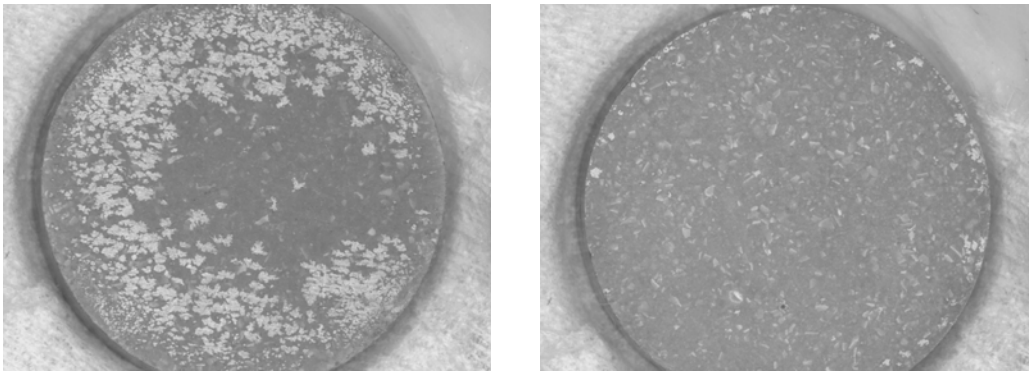

Sintered Surface Ground Surface

Figure 37. Optical micrographs of the as-sintered and the as-ground surfaces of a varistor pellet with 0.29 mol% Bi_2O_3, 300 ppm Na and a 50% green density after sintering at 725˚C for 16 hr in air and then cooling at 1.5˚C/min.

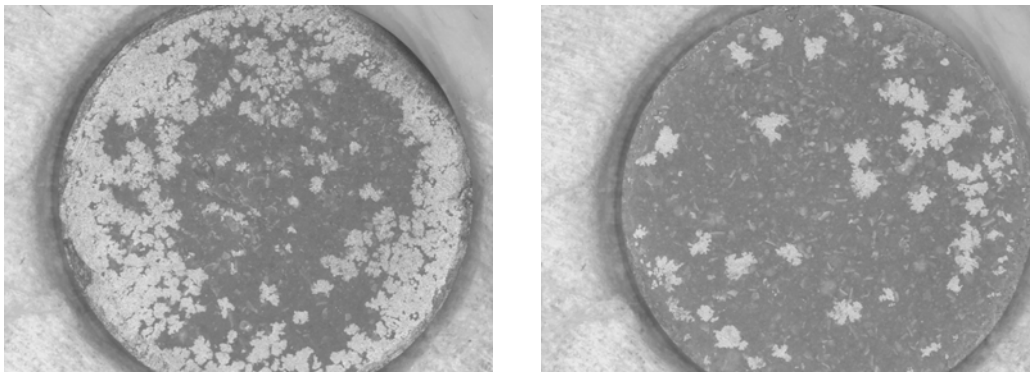

Sintered Surface Ground Surface

Figure 38. Optical micrographs of the as-sintered and the as-ground surfaces of a varistor pellet with 0.29 mol% Bi_2O_3, 300 ppm Na and a 55% green density after sintering at 725˚C for 16 hr in air and then cooling at 1.5˚C/min.

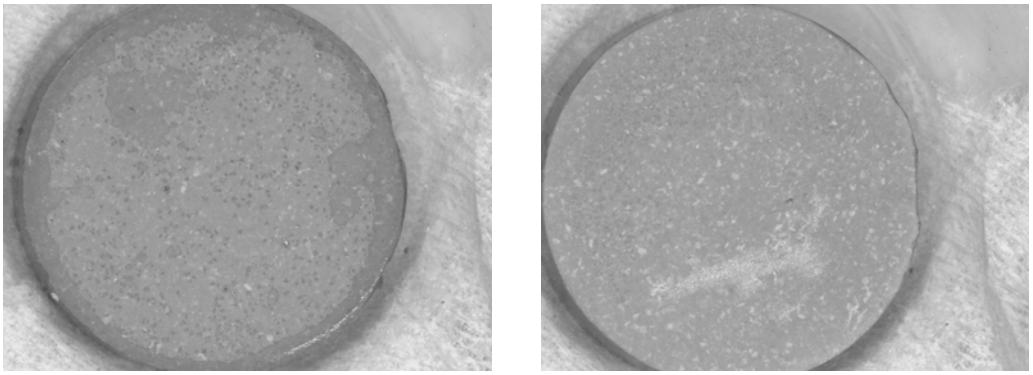

Sintered Surface Ground Surface

Figure 39. Optical micrographs of the as-sintered and the as-ground surfaces of a varistor pellet with 0.41 mol% Bi_2O_3, 300 ppm Na and a 40% green density after sintering at 725˚C for 16 hr in air and then cooling at 1.5˚C/min.

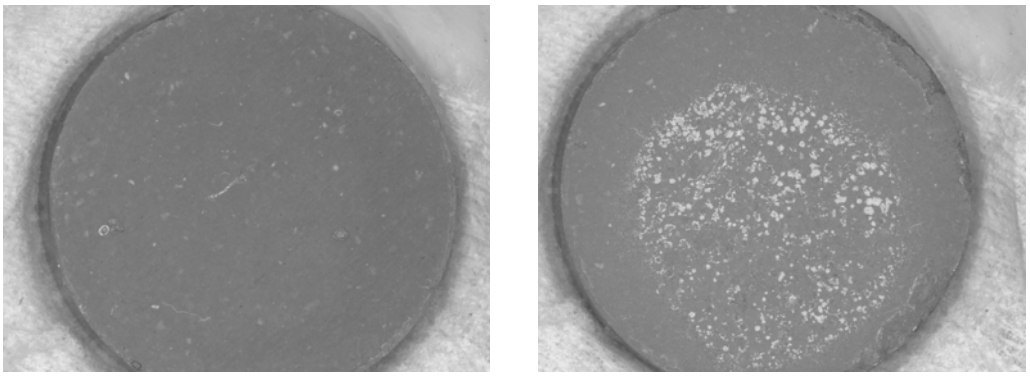

Sintered Surface Ground Surface

Figure 40. Optical micrographs of the as-sintered and the as-ground surfaces of a varistor pellet with 0.41 mol% Bi_2O_3, 300 ppm Na and a 55% green density after sintering at 725˚C for 16 hr in air and then cooling at 1.5˚C/min.

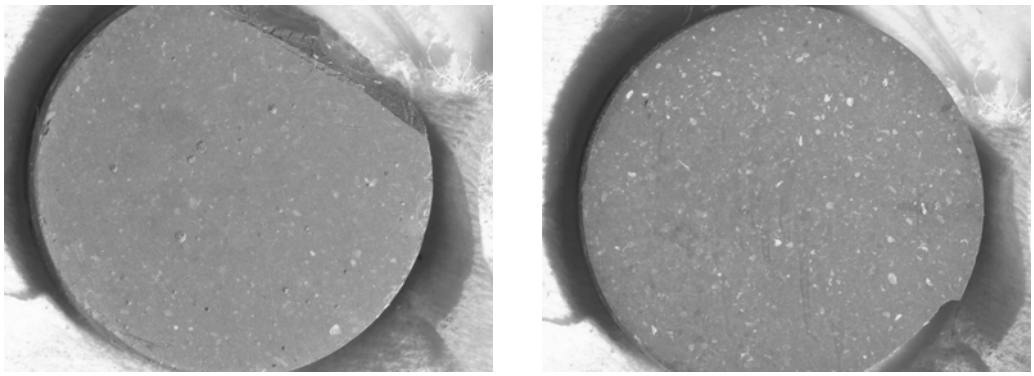

Sintered Surface Ground Surface

Figure 41. Optical micrographs of the as-sintered and the as-ground surfaces of a varistor pellet with 0.56 mol% Bi_2O_3, 300 ppm Na and a 50% green density after sintering at 725˚C for 16 hr in air and then cooling at 1.5˚C/min.

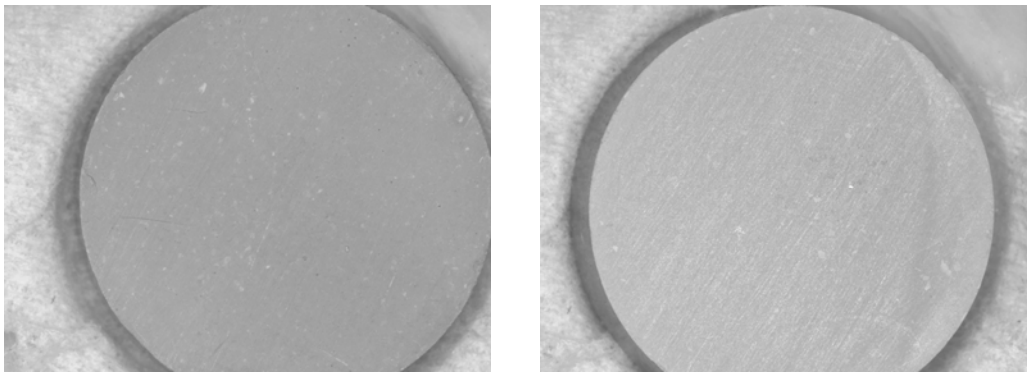

Sintered Surface Ground Surface

Figure 42. Optical micrographs of the as-sintered and the as-ground surfaces of a varistor pellet with 0.56 mol% Bi_2O_3, 0 ppm Na and a 50% green density after sintering at 725˚C for16 hr in air and then cooling at 1.5˚C/min.

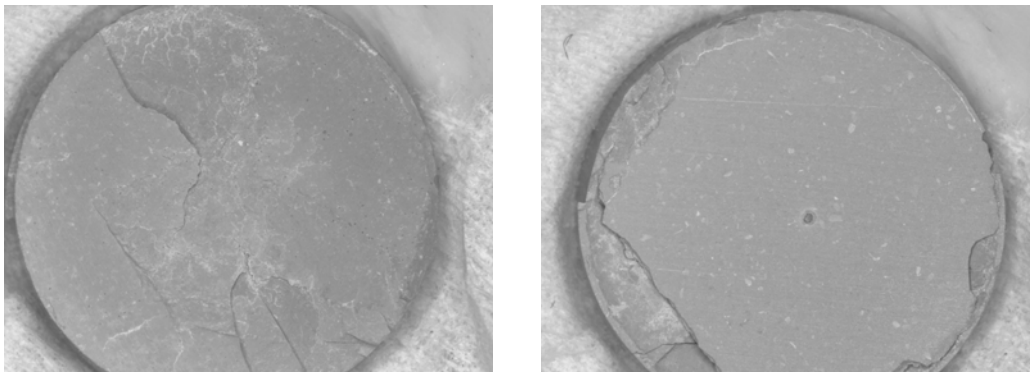

Figure 43. Optical micrographs of the as-sintered and the as-ground surfaces of a varistor pellet with 0.56 mol% Bi_2O_3, 0 ppm Na and a 55% green density after sintering at 725˚C for16 hr in air and then cooling at 1.5˚C/min.

Scanning electron micrograph images of some of the samples in Figs. 36 to 43 are shown in Figs. 44 to 57. The as-sintered and ground surfaces of the 0.27 mol% Bi_2O_3, 300 ppm Na, 55% green density sample are shown in Figs. 44 and 45, respectively. Numerous holes are seen to be present in the otherwise continuous bismuth oxide phase layer. The Bi_2O_3 phase appeared to have grains in the several micrometer range, while the grains of ZnO were under 1 μm. The edges of the Bi_2O_3 phase regions were generally much smoother on the as-sintered surface as compared to the ground surface where the phase regions are surrounded by partially covered areas where the phase present mainly between the ZnO grains. Fig. 46, from the as-sintered surface of a 0.29 mol% Bi_2O_3, 300 ppm Na, 55% green density sample, shows that the bismuth oxide phase can also contain cracks, which sometime follow the grain boundaries. Extreme differences in morphology between as-sintered and ground surfaces were also seen in the 0.41 mol% Bi_2O_3, 300 ppm Na, 55% green density sample as shown in Figs. 47 (as-sintered) and 48 (ground). In this case, the as-sintered surface had only small regions of the Bi_2O_3 phase, several micrometers in size that were tens of micrometers apart from each other. The ground surface had many large regions, some of which were continuous while others contained sparsely covered areas. At high magnification, ridges that appear to be growth fronts can be seen on some of the grains on the ground surface (Fig. 48). The as-sintered surface of the sample with standard composition and green density that had an atypical morphology of the surface phase is shown in Fig. 49. In this case, the bismuth oxide phase was in several larger, thick regions that were round in shape as well as in numerous isolated regions that were several micrometers in size. Also found in this

sample were some large masses of the bismuth oxide phase that appear to be erupting from the surface, as shown in Fig 50 in both secondary electron and back-scattered images. Fig. 51 shows two EDS spectra taken from a large, thick area of the bismuth oxide phase region (see insert picture). Both spectra have peaks for Zn in addition to Bi. The ground surface of this sample, Fig. 52, had only very small regions of the bismuth oxide phase. Note that the location of these regions did not correlate with the location of the pores.

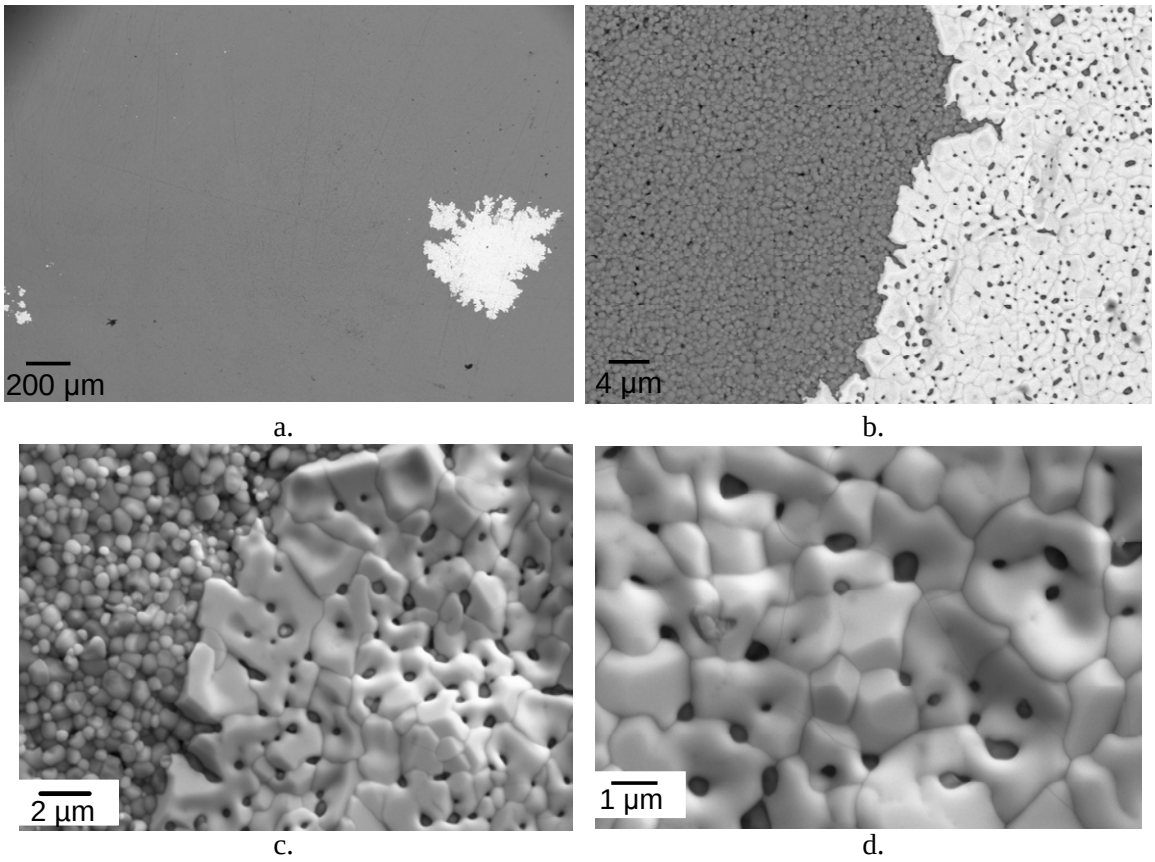

Figure 44. SEMs of the as-sintered surface of 0.27 mol% Bi_2O_3, 300 ppm Na, 55% green density sample after slow cooling: a. and b. are BSE and c. and d. are SE.

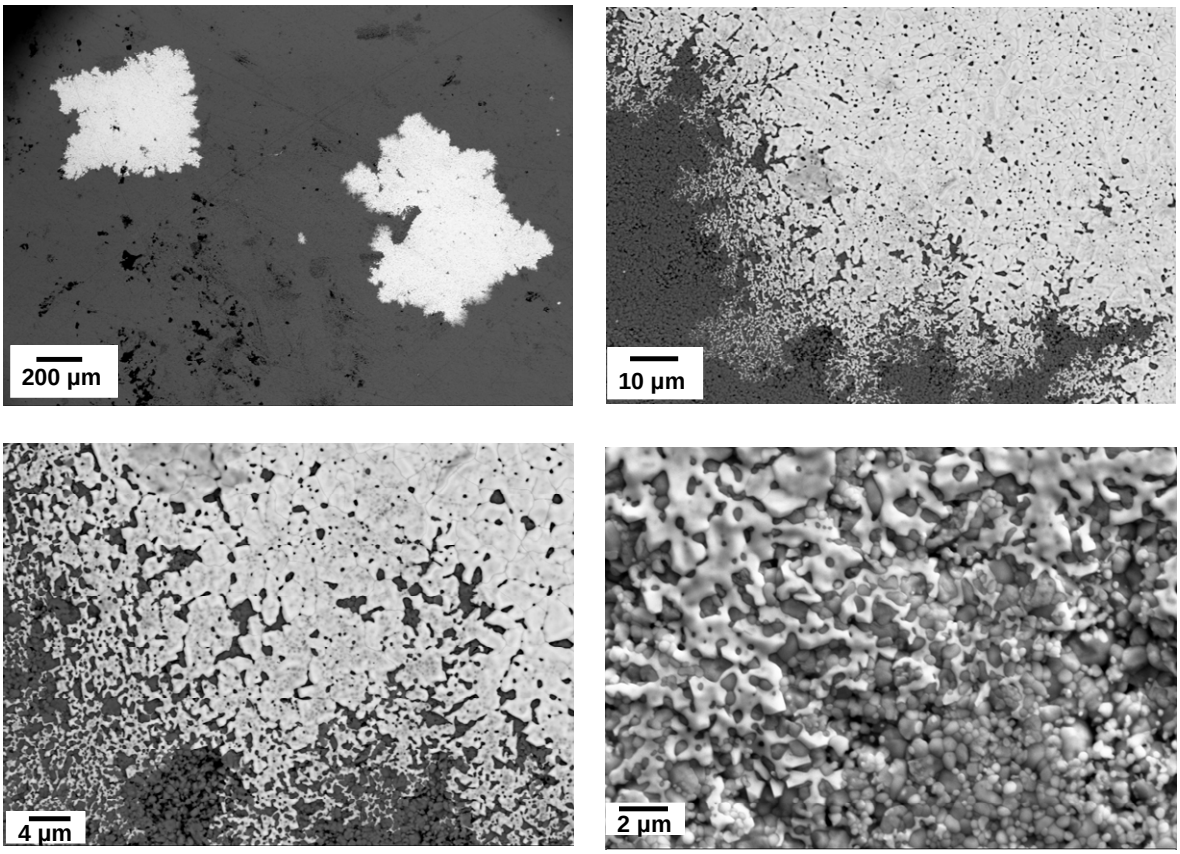

Figure 45. SEMs of the ground surface of a 0.27 mol% Bi_2O_3, 300 ppm Na, 55% green density sample after slow cooling: a. and b. are BSE and c. and d. are SE.

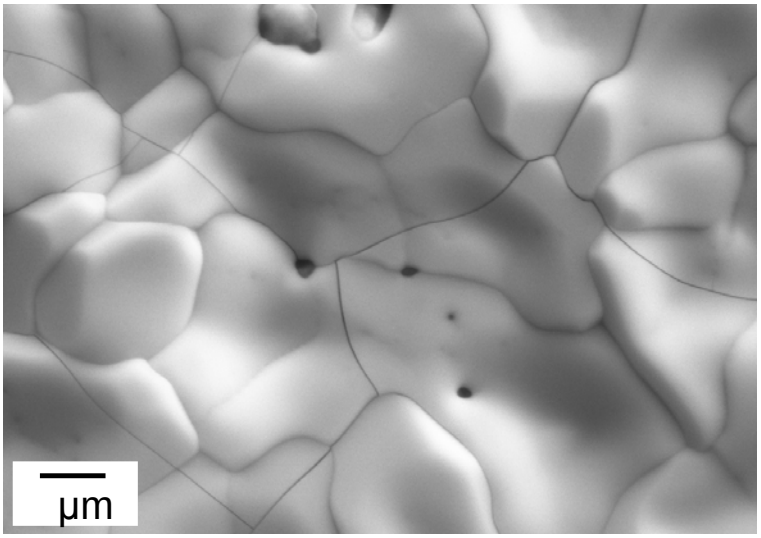

Figure 46. SEM (SE) of the as-sintered surface of a 0.29 mol% Bi_2O_3, 300 ppm Na, 55% green density sample after slow cooling.

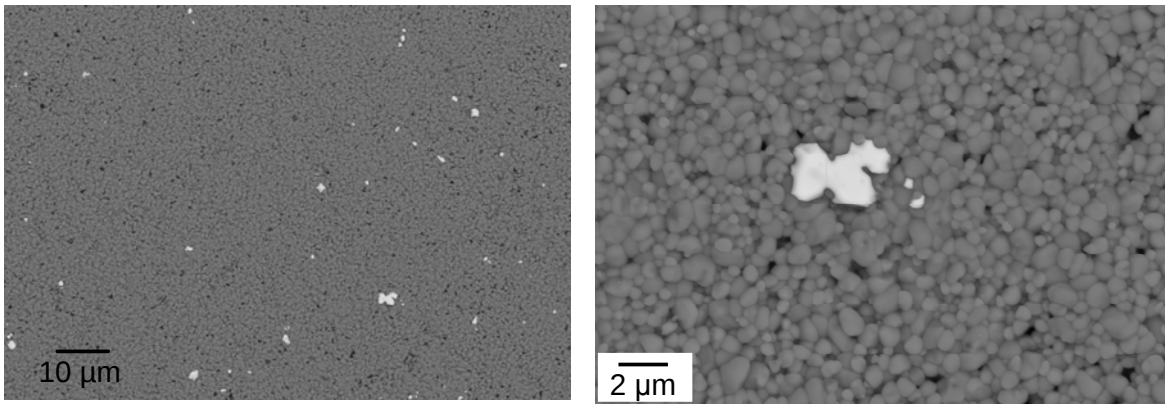

Figure 47. SEMs (BSE) of as-sintered surface of a 0.41 mol% Bi_2O_3, 300 ppm Na, 55% green density sample after slow cooling.

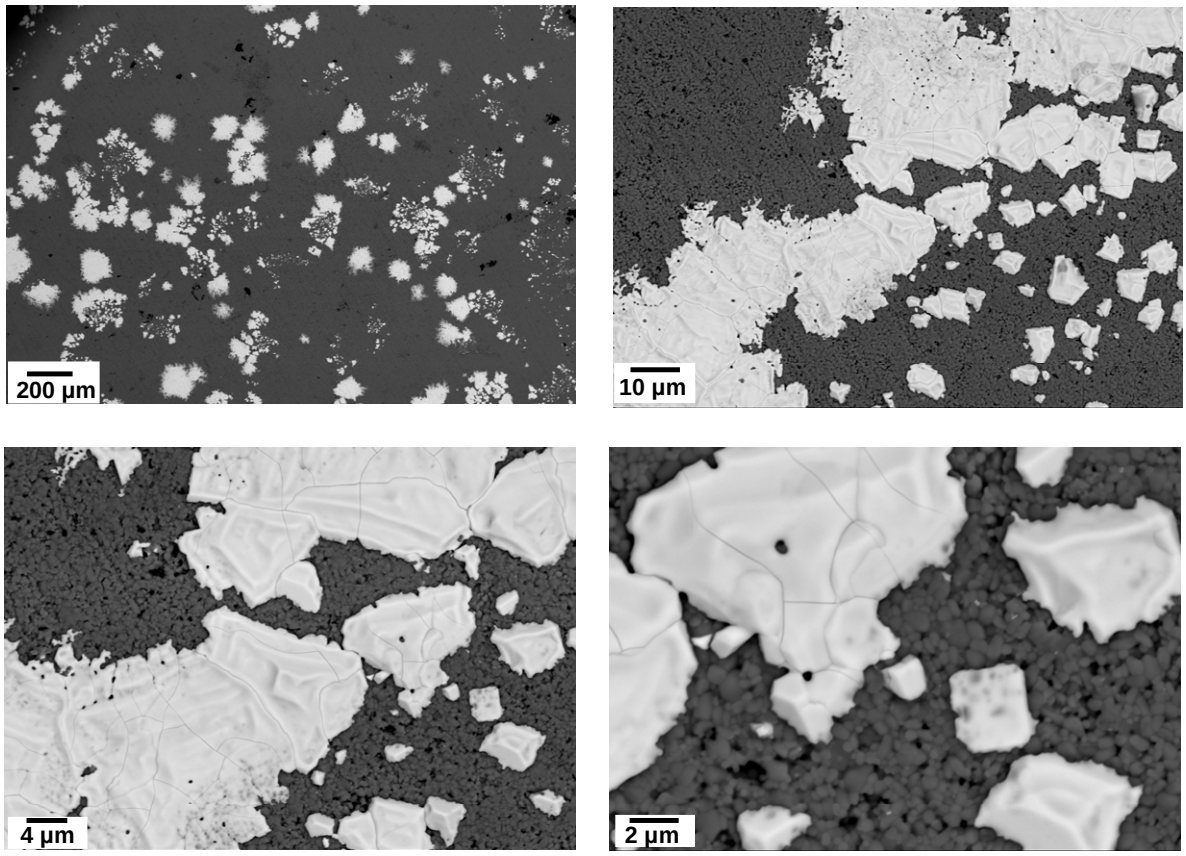

Figure 48. SEMs (BSE) of ground surface of 0.41 mol% Bi_2O_3, 300 ppm Na, 55% green density sample after slow cooling.

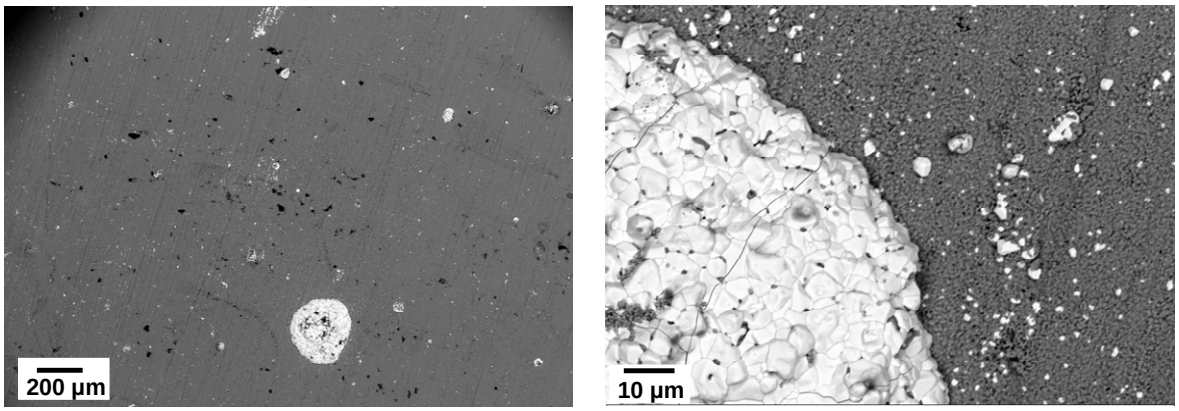

Figure 49. SEM images of the as-sintered surface of a 0.56 mol% Bi_2O_3, 300 ppm Na, 50% green density sample after slow cooling.

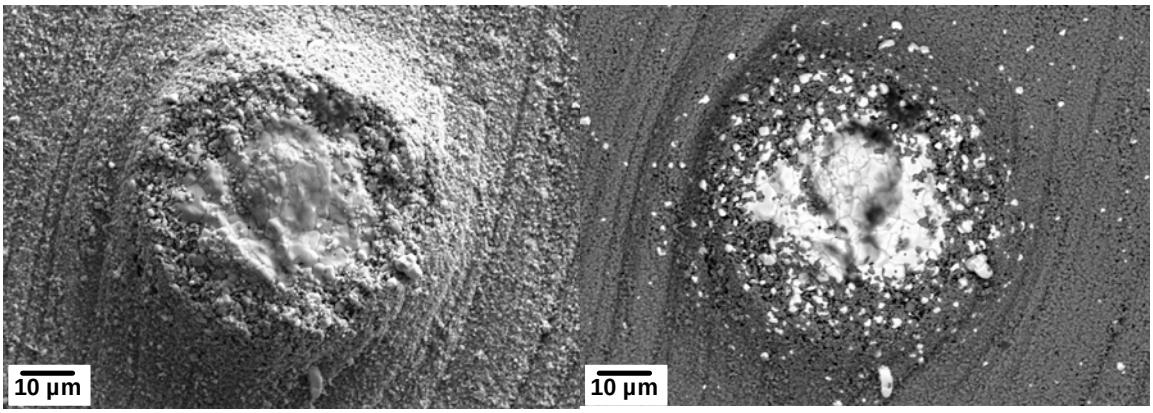

Figure 50. SEM images of the as-sintered surface of a 0.56 mol% Bi_2O_3, 300 ppm Na, 50% green density sample after slow cooling.

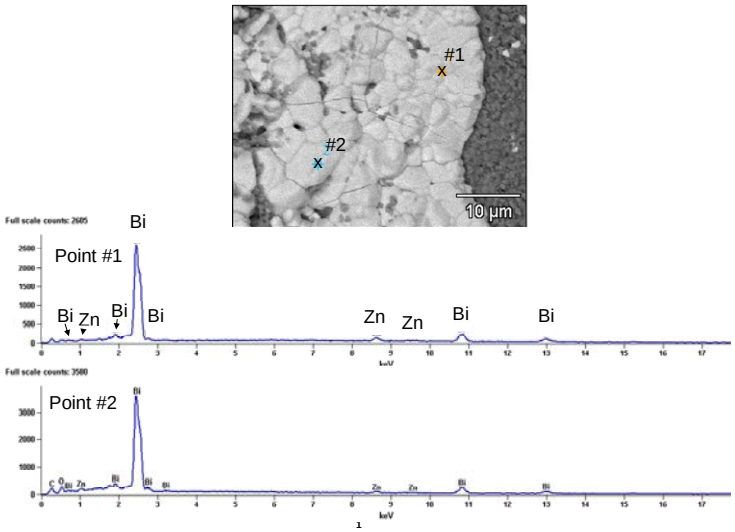

Figure 51. The EDS spectra taken at two locations in the bismuth oxide phase (shown in

the SEM image) of a standard composition varistor that had been slow cooled showing the presence of both Bi and Zn.

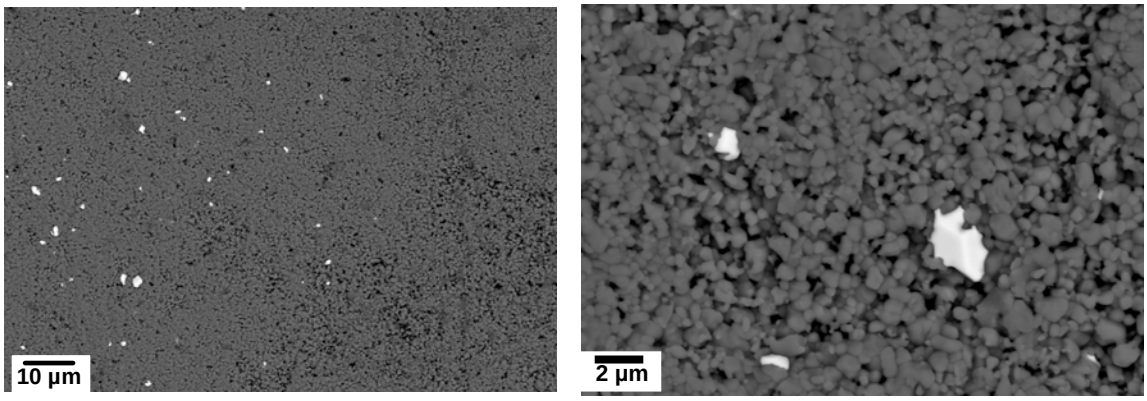

Figure 52. SEM images of the ground surface of a 0.56 mol% Bi_2O_3, 300 ppm Na, 50% green density sample after slow cooling.

The as-sintered and ground surfaces of a non Na-doped, 0.56 mol% Bi_2O_3 55% green density sample, Figs 52 and 53, respectively, were quite similar with a uniform distribution of mostly submicron specks of the bismuth oxide phase with a few larger regions. The larger regions on the as-sintered surface appear to be partly covered with ZnO particles, something not observed in the other samples.

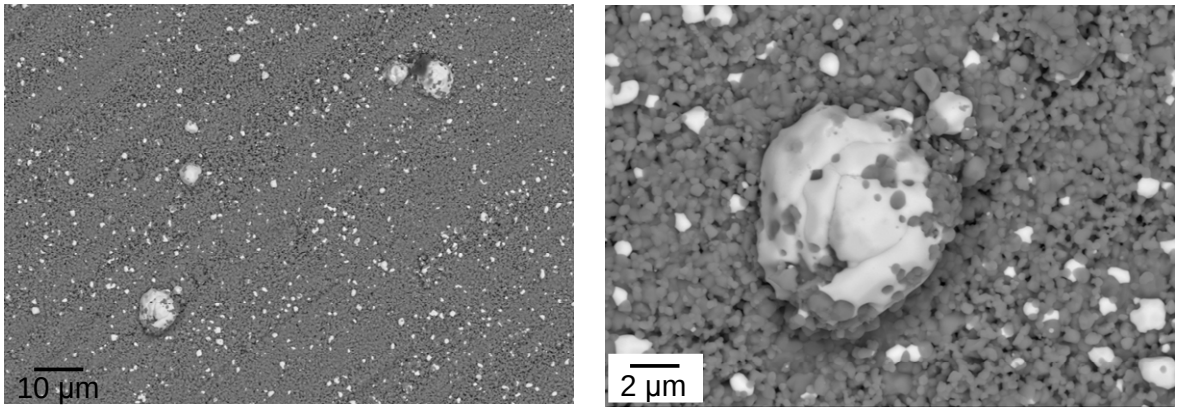

Figure 53. SEMs (BSE) of the as-sintered surface of 0.56 mol% Bi_2O_3, 0 ppm Na and 55% green density sample.

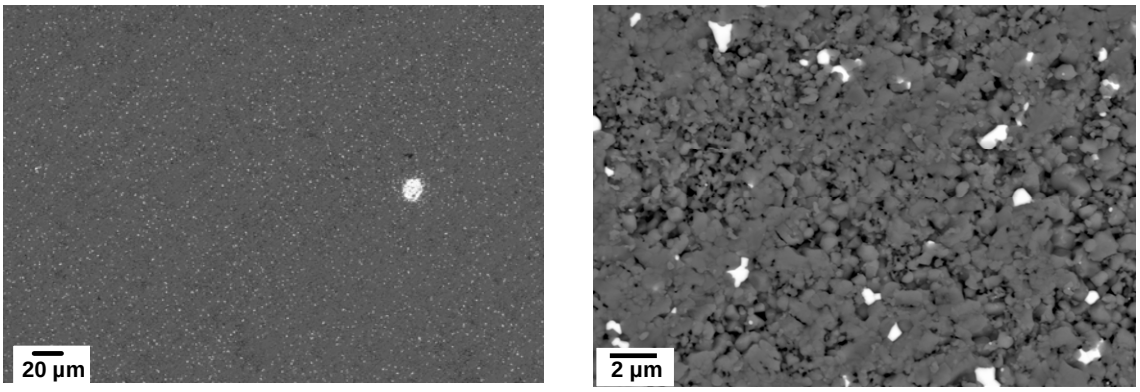

Figure 54. SEMs (BSE) of the ground surface of a 0.56 mol% Bi_2O_3, 0 ppm Na and 55% green density sample.

Figs. 55 and 56 are SEM images of the ground surface of a 0.41 mol % Bi_2O_3 sample with 300 ppm Na-doping that was originally sintered at 775˚C for 8.5 hr then cut into two pieces that were reheated to 750C and either slow cooled (Fig. 55) or quenched (Fig. 56). The slow-cooled sample had large regions of the bismuth oxide phase with edges where the phase was primarily in the ZnO grain boundaries. On the surface of the quenched sample, very tiny (~0.2 m) particles of the Bi_2O_3 phase are present scattered across the surface. Figs. 57 and 58 are SEMs of a sample with no Na doping (0.56 mol % Bi_2O_3) that was processed the same way as the samples in Figs. 55 and 56. In this case, the slow-cooled and the quenched halves had a similar distribution of the Bi_2O_3 phase but the slow-cooled sample (Fig. 57) had some slightly larger (2 - 3 μm) regions that were blocky and faceted as compared to those on the surface of the quenched sample (Fig. 58) that were smaller (1 - 2 μm) and had protrusions along ZnO grain boundaries. XRD patterns taken of these four samples are shown in Fig. 59. The only phases present were zincite and the $Bi_{38}ZnO_{58}$ phase. The lattice parameter of the $Bi_{38}ZnO_{58}$ phase was ~10.19Å for all the samples except the quenched half of the 300 ppm Na sample where it was 10.23Å

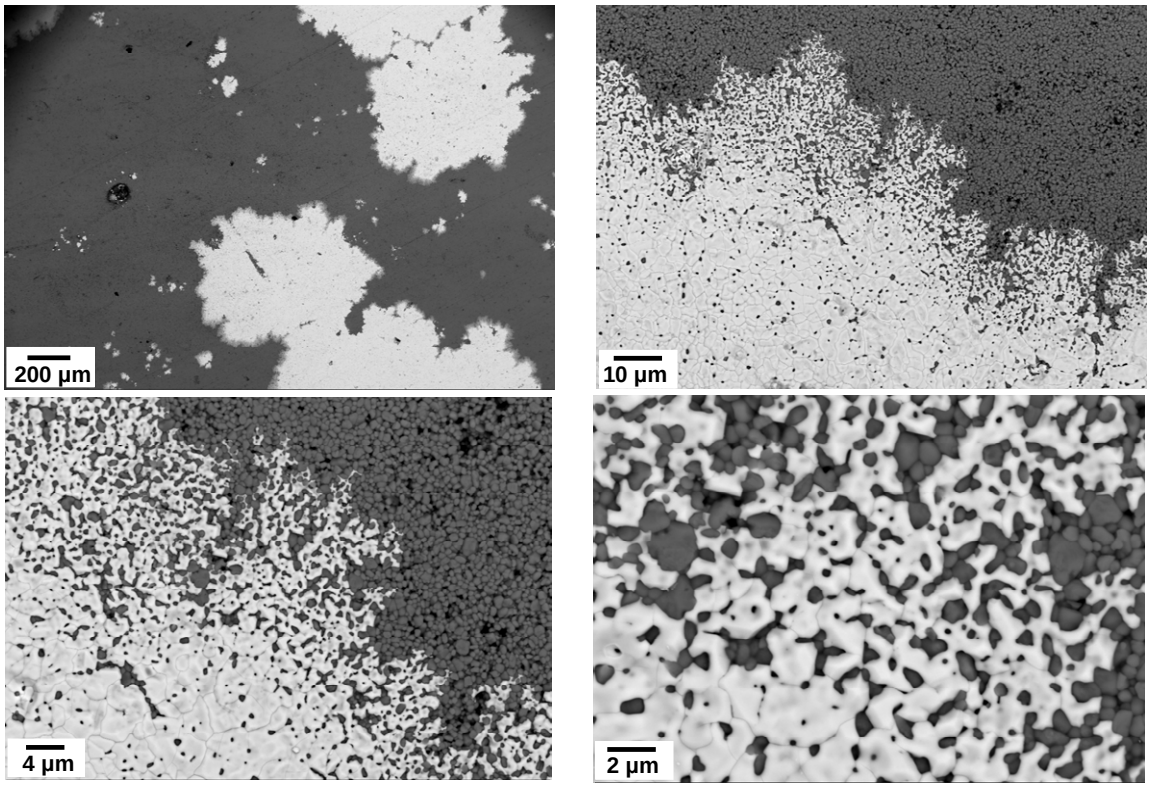

Figure 55. SEMs (BSE) of ground surface of 0.41 mol% Bi_2O_3 with 300 ppm Na sample after slow-cooling from 750˚C.

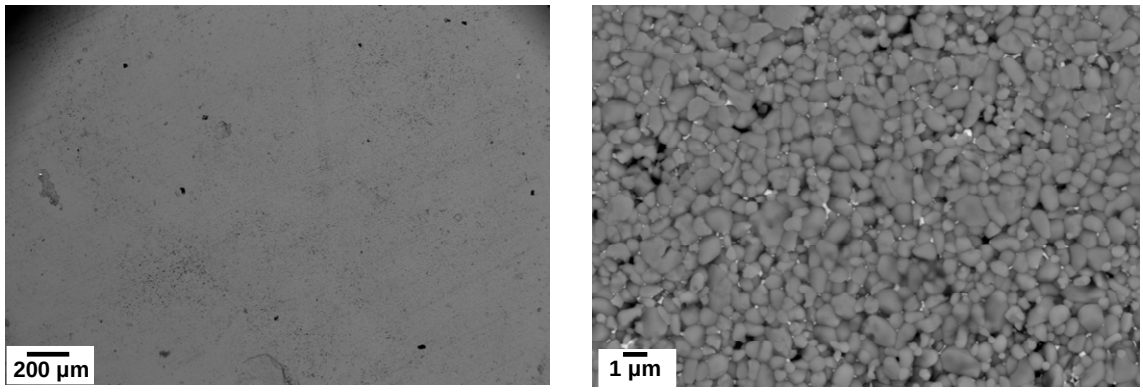

Figure 56. SEMs (BSE) of ground surface of 0.41 mol% Bi_2O_3 with 300 ppm Na sample after quenching from 750˚C.

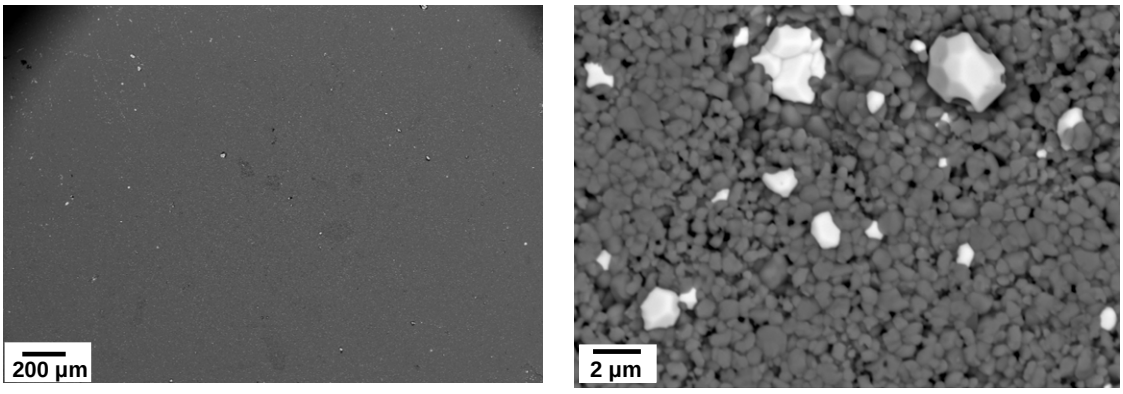

Figure 57. SEMs (BSE) of ground surface of 0.56 mol% Bi_2O_3 with 0 ppm Na sample after slow-cooling from 750˚C.

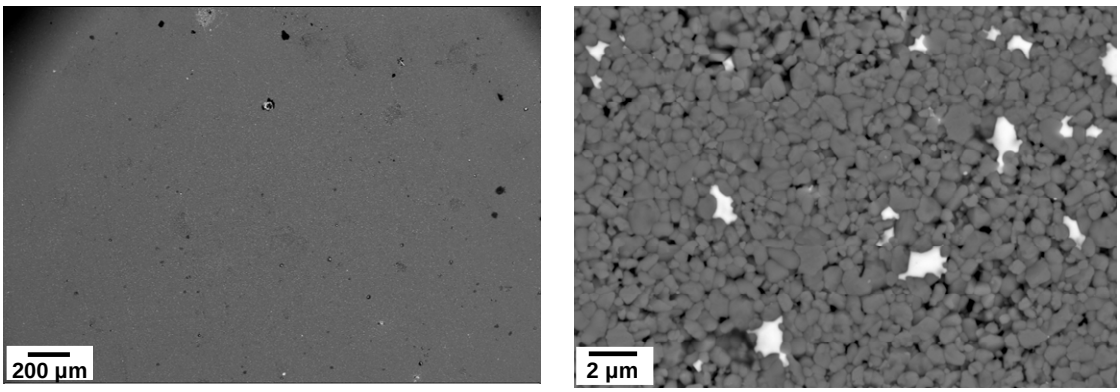

Figure 58. SEMs (BSE) of ground surface of 0.56 mol% Bi_2O_3 with 0 ppm Na sample after quenching from 750˚C.

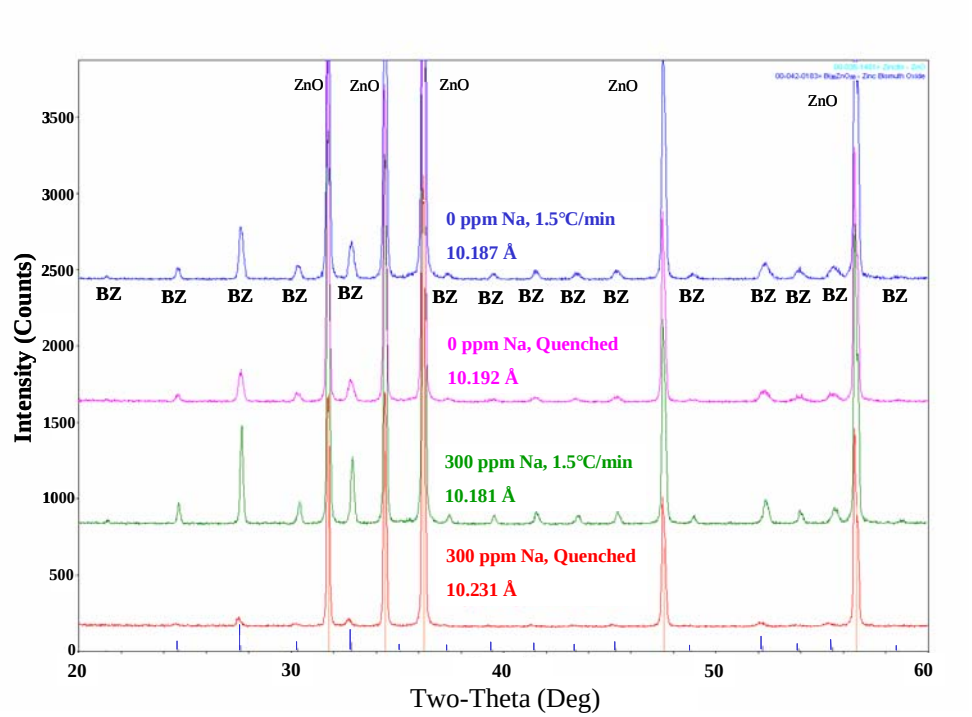

Figure 59. XRD patterns of the surface of the four varistor samples with and without Na-doping and either slow cooled or quenched that are shown in Figs. 55-58.

A series of *in situ* images taken during cooling at 1.5˚C/min of a standard composition varistor are shown in Fig. 60. This sample had previously been sintered for 16 hr at 750˚C and then the surfaces were ground with 600 grit SiC paper, prior to reheating in the video system furnace. No bismuth oxide phase regions have formed at 710˚C (the large bright areas in all the images near the center of the sample are reflections). By 701˚C, a large number of uniformly sized round regions of the bismuth oxide phase have nucleated on the surface. By 693˚C, most of the nuclei have grown and become somewhat irregular in shape. Very few new nuclei have appeared. These trends continue with further cooling until 653˚C, below which no further changes were noted.

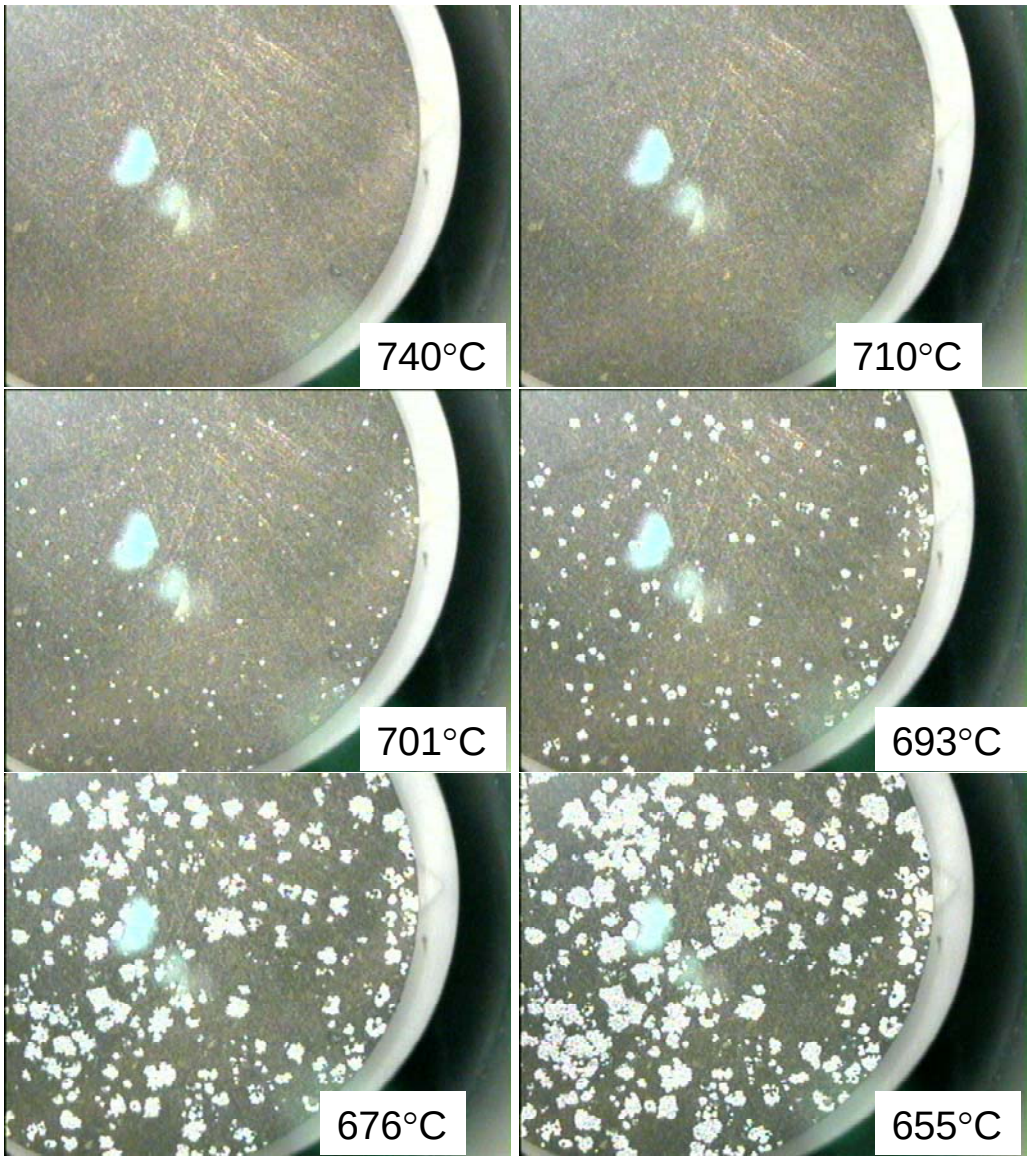

Figure 60. *In situ* images of a pre-sintered, standard composition varistor pellet (~1 cm in diameter) during cooling in flowing air at 1.5˚C/min.

Fig. 61 shows *in situ* images during reheating of a standard composition, pre-sintered varistor sample that had been slow cooled so that the bismuth oxide phase regions formed on the surface. Between room temperature and 577˚C, no changes are observed in the morphology of the regions, but by 658˚C the regions have shrank noticeably in size. By 679˚C, many of the smaller regions have disappeared and the larger ones appear to be sinking into the interior of the sample. Nearly all the bismuth oxide phase is gone by 710˚C and by 735˚C the last small regions have vanished. The sample was heated to 750˚C and then cooled at 1.5˚C/min (see Fig. 62). In this case the first sign of the bismuth oxide phase was observed at 685˚C with growth seen down to

645˚C. The number of the regions was much smaller than were originally present on this area of the sample and there little or no overlap in the location of the regions before and after the reheating, as is shown in Fig. 63.

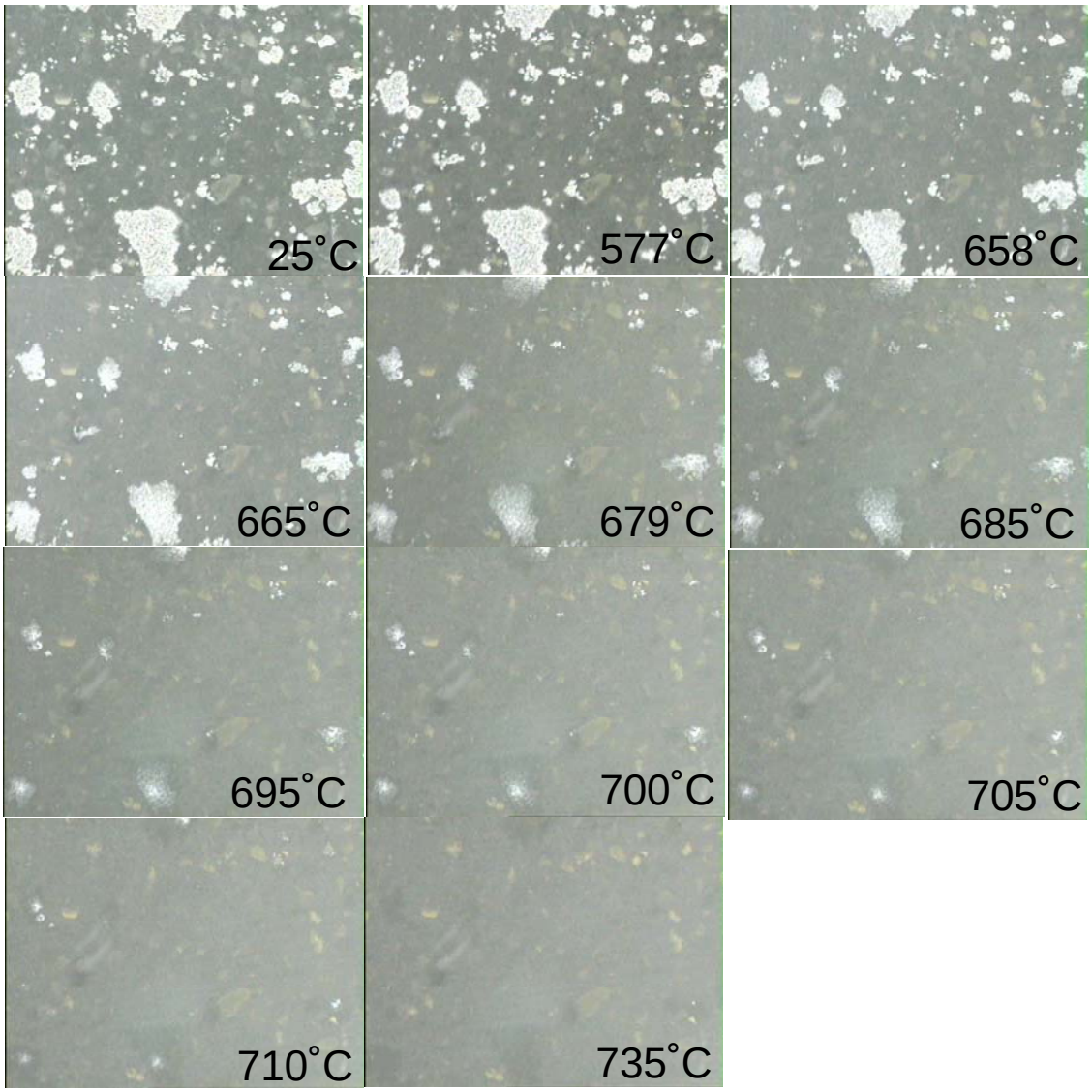

Figure 61. *In situ* images of a pre-sintered, standard composition varistor that had been slowly cooled during reheating in flowing air at 1.5˚C/min.

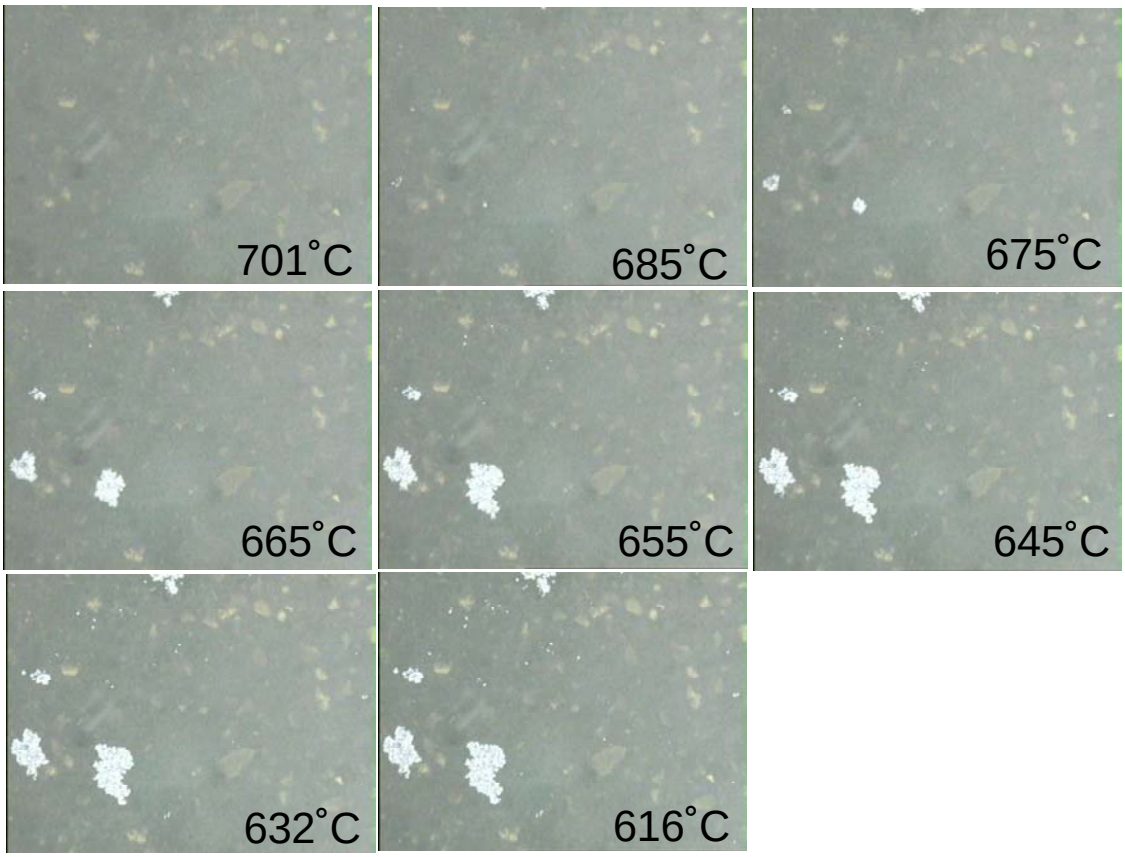

Figure 62. *In situ* images of the same region of the same sample in Fig. 64 during subsequent slow cooling in flowing air at 1.5˚C/min.

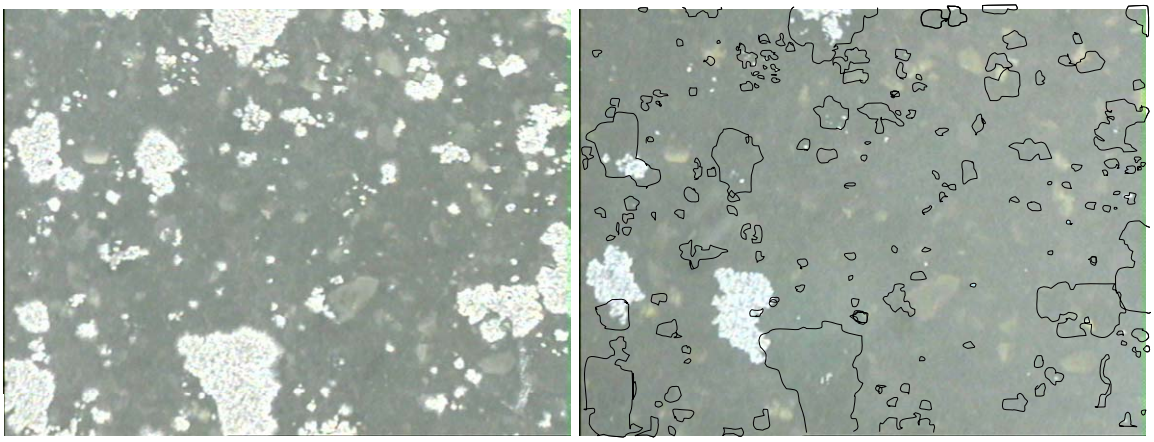

Figure 63. A comparison of the same region of the sample in Fig. 64 and 65 prior to (left) and after slow reheating and cooling (right). Outlines of the original bismuth oxide phase regions are drawn on the final image to aid in comparison.

Fig. 64 shows the results of the *in situ* XRD performed on a sample of green standard composition material that had been pressed to form a pellet and then crushed and spread in a thin layer on a thin alumina substrate. Initially and during heating to 300˚C, bismuthite, $Bi_2O_3 \cdot CO_2$, is

present (labeled with “C”). Also present at this and all other temperatures were zincite (not shown) and alumina (“A”) that was from the alumina substrate. By 400˚C, the bismuthite had decomposed and β-Bi_2O_3, the metastable tetragonal phase, had formed. This phase persisted until 650˚C where the peaks labeled “BZ” for the Bi_2O_3–ZnO binary phase appeared. Interestingly, this phase was definitely still present at 800˚C and possibly even at 825˚C, although the intensity of its peaks decreased markedly above 775˚C. During cooling, shown on the right, the binary phase is the only bismuth-containing phase seen and it seems to increase in intensity at 775C, similar to what was seen during heating.

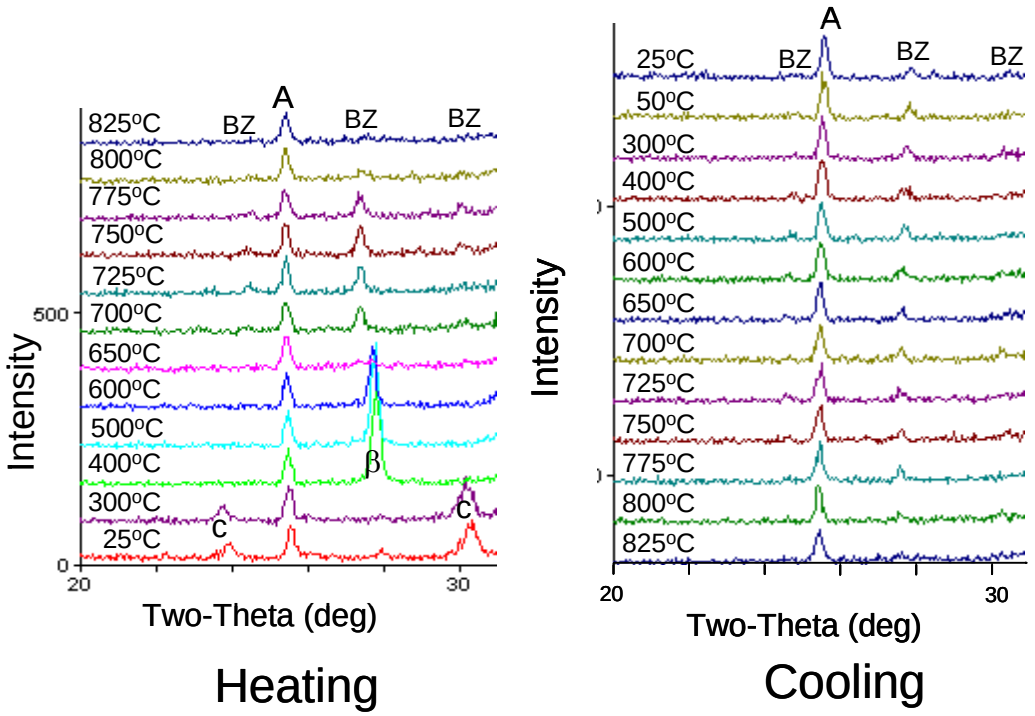

Figure 64. XRD patterns taken during heating and cooling of a thin layer of a crushed pellet of standard composition material that had not previously been sintered.

The results of the *in situ* XRD of a previously sintered and then slow-cooled standard composition pellet are shown in Fig. 65a during reheating and then cooling. In this case too the only Bi phase was the binary phase and it persisted to the highest temperature studied, 750˚C, although its intensity decreased above 700˚C. To avoid the effect of the binary phase retracting into the pellet, a second sample of sintered standard material was analyzed during heating after it was crushed and formed into a thin layer on an alumina substrate, see Fig. 65 b. In this case, the binary phase was once again seen up to 800˚C, with a decrease in intensity at 775˚C.

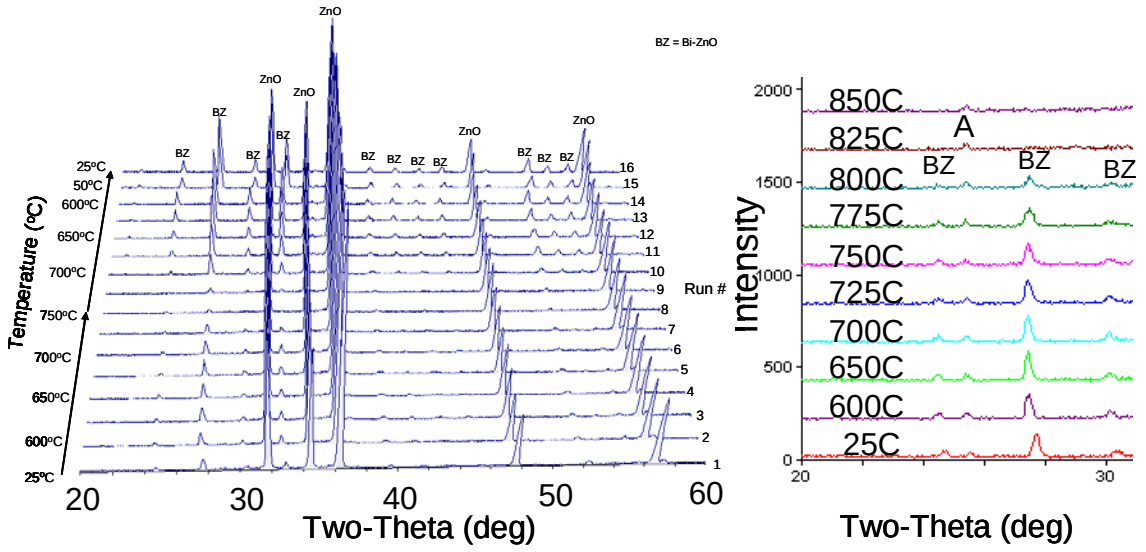

a. b.

Figure 65. XRD patterns of a previously sintered standard composition material during heating and cooling in pellet form (a.) and during heating after crushing (b.).

5.0 Discussion

5.1 Densification Behavior

The sintering experiments on the DOE samples (Fig. 2) showed that the low bismuth oxide samples not only densified to a lesser degree at a given temperature than the 0.56 mol% samples, as expected, they also were affected to a much greater extent by the other variables. All of the high Bi_2O_3 samples were between 90 and 92% of theoretical density at 740˚C whereas the range was 81 to 92% for the low Bi_2O_3 samples at 780˚C. This was largely due to the much greater effect of Na doping on the densification of the low Bi_2O_3 samples. The stronger effect for low Bi_2O_3 content samples could be related to how the sodium affects the spreading of the grain boundary phase throughout the material (see Figs. 44 - 54). This is likely more important when the content of bismuth oxide is close to the minimum amount necessary to cause densification. The low Bi_2O_3 samples with standard mixing and high Cl content (only 7 washes) behaved somewhat anomalously, in that they had lower than expected densities at low sintering temperatures and higher than expected densities at higher temperatures. Also, the sintering atmosphere was shown to have a small but measurable effect on the densification behavior of the DOE samples with higher density in the 5 to 10% range being reached in argon as opposed to air or oxygen (see Figs. 4 - 6.). The enhancement came during the initial stage of sintering during

heating and was then maintained at about the same level throughout the isothermal hold. The low oxygen pressure could be increasing the mobility of oxygen in the grain boundary phase or possibly aiding this phase's formation or distribution along the boundaries. More work is needed to determine which, if any, of these explanations is correct.

The effect of the bismuth oxide content on densification can be seen more clearly in Figs. 14 to 17 and 19 to 22. In agreement with Gardner *et al.*, samples with low bismuth oxide contents would begin to densify only after the first several hours of the isothermal hold at 775˚C and below. Based on the mottled appearance of the samples as they began to densify (Fig. 18), this behavior appeared to be related the formation of regions of higher and lower bismuth oxide content. In a manner similar to the way that the sodium content greatly influences the formation of bismuth oxide phase rich regions on the surface, the sodium may help to form the bismuth oxide rich regions that start the densification process. This would explain the enhancement in densification seen in sodium-containing samples and why the effect of Na is strongest at low bismuth oxide contents. It is also consistent with the behavior of samples with various amounts of sodium and 0.56 mol% Bi_2O_3 (Figs. 25 to 32) where the largest effect of the sodium level is seen around 700˚C, the temperature where the surface regions disappear. More work is needed to better understand this mechanism.

Returning to the effects of bismuth oxide concentration, a temperature of ~725˚C is required to produce samples with densities >90% in a reasonable amount of time (~15 hr) and at this temperature, there is little effect of Bi_2O_3 content on density for contents ≥0.41 mol%. At 750˚C the behavior is similar except that only ~5 hr is required to reach >90% density. At 775˚C all the samples, except the one with 0.25 mol%, reach >90% density by 2 hr and at 800˚C in ~1 hr. Previous work[30] on non-Na doped Sandia material with 0.56 mol% Bi_2O_3 showed that the electrical requirements could be met with temperature-time combinations similar to those that gave ~90% density. Determining whether or not switching field requirements could be met for the lower Bi_2O_3 levels with sodium doping would be of interest.

5.2 Sample Size Effects on Densification and Mass Loss

Experiments with DOE samples of various sizes and shapes cut from the same slug clearly showed that both the densification and the mass loss vary with the ratio of the surface area to the

volume of the sample (Figs. 7 - 11). Larger, lower SA/Vol samples densified to a greater extent and lost less mass. The fact that some bismuth oxide vaporizes at these relatively low temperatures (as confirmed by the stain left on the alumina setter shown in Fig. 13) is interesting since other workers have found this degree of mass loss occurs at approximately 300˚C higher temperatures.[26] However, the mass loss measured tended to increase linearly with the SA/Vol ratio over the range studied while the density increase was observed primarily as SA/Vol decreased below 1 mm^{-1}. Instead of being directly caused by the loss of bismuth oxide, the enhancement in densification could very well be due to how the oxygen partial pressure inside the pores of the sample is affected by sample size. As a varistor sample begins to sinter, the bismuth oxide phase at the grain boundaries may remove oxygen from the atmosphere in the pores, since studies have found excess oxygen at varistor grain boundaries. In samples sintered in air with at least one small dimension, such as the plates or rods, oxygen can flow from the surface through the pore network to replace much of the lost oxygen. The additional oxygen may lower the oxygen diffusion rate through the bismuth oxide grain boundary phase by decreasing its oxygen vacancy concentration thereby decreasing the rate of densification. This is consistent with the results discussed above (Figs. 4 - 6) that showed enhanced densification in an argon atmosphere compared to air or oxygen and with the results in Table 2 that showed a crucible-covered sample densified more than a comparable sample that was setting uncovered on its edge that could interact more readily with the atmosphere. Further, the range of SA/Vol values where the steepest change in density occurred was ~0.5 mm^{-1}, which corresponds to a cube ~12 mm or 0.5” on a side. This dimension is comparable to the thickness of a slug where a decrease in α has been reported. This technologically important hypothesis could be tested by sintering large and small cubes in oxygen and in argon to see if the size effect on densification is eliminated. Further, the α of the large oxygen-sintered samples could be measured to determine if there is a change in regulation capability.

5.3 Bismuth Oxide Phase Behavior

Room temperature XRD results (Fig. 59) on slow-cooled samples with both standard and no Na-doping indicate that the bismuth oxide is present as the $Bi_{38}ZnO_{58}$ phase. This identification is made based on the lattice parameter since the crystal structure of $Bi_{38}ZnO_{58}$ is the same as that of γ-Bi_2O_3. The EDS results (Fig. 51) confirmed the presence of Zn in the bismuth oxide containing

phase that was on the surface of a slow-cooled sample with 300 ppm Na. However, the lattice parameter measured for a quenched sample with 300 ppm Na (10.231Å) was midway between that of γ-Bi_2O_3 (10.261Å) and that of $Bi_{38}ZnO_{58}$ (10.201Å).

The *in situ* XRD of unsintered powder indicated that the bismuth was in the form of the oxycarbonate bismuthite, $Bi_2O_3 \cdot CO_2$, from room temperature to above 300˚C (Fig. 64). By 400˚C, the bismuthite had transformed to the metastable tetragonal phase β-Bi_2O_3. The formation of β-Bi_2O_3 from bismuthite was reported by Levin and Roth.[53] By 650˚C, the β phase has disappeared and the $Bi_{38}ZnO_{58}$ has begun to form. This is the same temperature range where densification starts. Fig. 3 shows that shrinkage of standard composition material does not begin densifying during heating at 5˚C/min until between 675˚ and 700˚C, but densification does gradually occur at 650˚C with heating for several hours as is shown in Fig. 14. Thus it seems that the formation of the binary phase is a necessary but not a sufficient condition for densification. In addition, it appears that once this phase is formed, time is required for it to spread along the grain boundaries or possibly for the amorphous solid phase found by Luo *et al.*[30] to form from the binary phase. However, if an amorphous solid does form, it must contain a relatively small fraction of the bismuth oxide present since there was no decrease in the intensity of the XRD peaks of the binary phase until much higher temperatures.

Surprisingly, the high-temperature XRD results on both previously unsintered powder and on reheated sintered material in pellet (Fig 65a) or crushed powder form (Fig. 65b) indicated that the binary phase remains present to temperatures above 800˚C, well above the eutectic temperature of ~738˚C. For the powdered samples, the intensity of the peaks for the binary phase do not decrease until above 750˚C although a decrease did occur above 700˚C for the previously sintered pellet, most likely do to the loss of the bismuth oxide phase on the surface that occurs in this range (see Fig. 61). According to all the published equilibrium phase diagrams, all of the binary phase should abruptly melt at eutectic leaving only zincite plus liquid. Either the phase diagrams are incorrect or equilibrium is not maintained in the varistor microstructure for some reason. Since significant sintering occurred at 650˚C (Fig. 14) and densities >90% were reached at 725˚C (Fig. 17), a eutectic liquid is not necessary for sintering to occur and a significant amount of liquid does not form until >750˚C, well above the normal varistor sintering temperatures used at Sandia.

The formation and morphology of the bismuth oxide containing phase on the surface of sintered varistors was studied for several reasons. Similar regions internal to the varistor samples also exist but their formation cannot be directly observed. The behavior of this material on the surface as a function of composition and temperature can provide clues about this phase, which is critical to the densification and electrical properties of the varistors. These regions were found to form during the slow cooling of well-sintered, sodium-doped samples from nuclei that form ~700˚C and continue to grow until ~650˚C (see Fig. 60). During reheating, the process happens in reverse (Fig. 61) and subsequent re-cooling leads to the formation of new regions in different locations (Fig. 62). According to the high-temperature XRD results, the bismuth oxide is in the crystalline binary phase when these processes are occurring. The growth process of the large regions may very well involve vapor phase transport.

The overall morphology of the regions varies considerably (Figs. 36 to 41) from sample to sample, even for samples with the same composition and heat treatment, and on the surface condition of the same sample. SEM images (Figs. 44, 45 and 55) reveal that growth of the regions involves moving first along the zinc oxide grain boundaries and leaving holes above the center of zinc oxide particles after the material along the boundaries thickens and joins up with material from nearby boundaries. It seems likely that the presence of grain boundary grooving on the as-sintered surfaces is what causes the regions on them to grow differently from those on the ground surfaces. The fact that the material is generally cracked (Fig. 46) indicates that it has a higher coefficient of thermal expansion than does the zinc oxide. Lattice parameters measured during the high temperature XRD scans confirmed this. Without sodium doping (Figs. 53 and 54), the binary phase regions were mostly small (0.5 to 2.0 μm) with little difference between as-sintered and ground surfaces. A possible reason that the presence of sodium causes the large regions to form is that it greatly decreases the formation of nuclei by altering the surface and/or grain boundary energies so that the few nuclei that form grow large. This is consistent with the fact that the quenched non Na-doped sample had many micron-size binary phase particles present (Fig. 58) whereas, the fewer particles present on the quenched Na-doped sample were extremely small, ~0.1 μm (Fig. 56).

A clearer picture of the sintering process of the Sandia chem-prep high field varistor material can be formed by combining all the results of this study. The first step in the sintering process appears to be the formation of the $Bi_{38}ZnO_{58}$ phase from the β-Bi_2O_3 phase around 650˚C. The binary phase has an appreciable vapor pressure in the normal range of sintering temperatures, leading to mass loss that depends on sample size and most likely providing a mechanism of mobility for the phase to redistribute itself. The distribution of this phase must then occur for densification to commence. This occurs readily with >~0.4 mol% Bi_2O_3 and seems to be facilitated by the presence of the sodium. This phase, when at the grain boundaries, provides the enhanced oxygen diffusion pathways, possibly forming some amorphous phase. However, a eutectic liquid does not appear to form, since that would imply the complete disappearance of the crystalline phase that *in situ* XRD showed was still present at much higher temperatures. Densification is enhanced in a low oxygen atmosphere, either by using an inert gas atmosphere or, as sample size increases, by the low oxygen atmosphere created inside the sample as excess oxygen goes to the grain boundaries. Increased oxygen mobility in the grain boundary phase at low pO_2 is thought to cause this phenomenon. A relative density >90% of theoretical can be reached at ~700˚C or higher in a reasonable amount of time. This temperature corresponds to the temperature where the binary phase surface regions fully disappear so that this phase is completely spread out at the grain boundaries. During slow cooling, these regions nucleate on the surface at 700˚C, in Na-doped samples, that then continue to grow until ~650˚C, in a process that occurs when the material is fully crystalline and seems to be driven by surface and interfacial energies, not thermal expansion mismatch.

6.0 Summary

The results of this study are summarized in the following points:

1. The impact on densification of the presence of the Na was much larger for low bismuth oxide samples (0.30 mol%) than for samples with the standard amount.
2. Sintering in argon increases the final density by 2 to 6% for standard composition varistors and by even more for some lower bismuth oxide compositions.
3. Large samples (SA/Vol < 0.5 mm^{-1}) can have up to ~6% higher volume shrinkage during sintering than smaller samples (SA/Vol > 1.0 mm^{-1}).
4. Samples lose mass (bismuth oxide) depending linearly on their SA/Vol ratio from 0.4% when SA/Vol = 0.5 mm^{-1} to 1.0% when SA/Vol = 4.5 mm^{-1}.

5. The densification behavior of samples with 0.56 and 0.48 mol% Bi_2O_3 with 300 ppm Na was very similar at all temperatures studied (650˚C to 825˚C) and the behavior of 0.41 mol% Bi_2O_3 samples was similar to these at 750˚C and above.
6. At low temperatures, low bismuth oxide samples either did not densify (0.25 mol% at 700˚C and below) or densified only after a long induction period (0.25 mol% at 725˚C and 0.33 mol% at 650˚C).
7. The time required to reach ~90% density for samples with 0.41 mol% Bi_2O_3 or greater and 300 ppm Na decreases from ~14 hr at 725˚C to 5 hr at 750˚C and to ~2 hr at 775˚C.
8. The densification of samples with 0.56 mol% Bi_2O_3 generally increased with the level of Na present by ~5% between 0 and 600 ppm except around 700C where the effect was much stronger, ~20%.
9. During sintering, the bismuth oxide transforms from an oxycarbonate, bismuthite, to the metastable tetragonal phase of Bi_2O_3 by 400˚C which remains present until above 600˚C.
10. By 650˚C, the β-Bi_2O_3 has disappeared and the binary $Bi_{38}ZnO_{58}$ phase has started to form, the presence of which is required for sintering to commence.
11. The bismuth oxide remains crystalline as $Bi_{38}ZnO_{58}$ to >800˚C, although by 775˚C the amount of it has diminished somewhat, indicating that a eutectic liquid is not present during normal varistor sintering.
12. The bismuth oxide phase reversibly forms large regions on the surface during slow cooling at ~700˚C for samples with 300 ppm Na but these regions do not form on samples that are not Na-doped.
13. The $Bi_{38}ZnO_{58}$ surface regions grow from the nuclei that form ~700˚C and continue to grow until ~650˚C.
14. The $Bi_{38}ZnO_{58}$ surface regions do not reform in the same locations on the surface of a sample that was heated well above 700˚C and then slow cooled.
15. The structure and morphology of the surface regions is affected significantly by the roughness of the surface, the density of the sample, and other unknown factors.

7.0 References

[1] R. G. Dosch and K. M. Kimball, “Chemical preparation of high-field zinc oxide varistors,” Sandia National Laboratories Report SAND85-0195, 1985.

[2] T. J. Gardner and S. J. Lockwood, “Scale-up of a batch-type chemical powder preparation process for high field varistor fabrication,” Sandia National Laboratories Report SAND87-2194, 1988.

[3] K. M. Kimball and D. H. Doughty, “Aluminum doping studies on high field ZnO varistors,” Sandia National Laboratories Report SAND86-0713, 1987.

[4] J. W. Medernach, R. L. Snyder, “Powder diffraction patterns and structures of the bismuth oxides,” *J. Am. Ceram. Soc.* **61**, 494–497 (1978).

[5] H. A. Harwig and A. G. Gerards, “The polymorphism of bismuth sesquioxide,” *Thermochimica Acta* **28**, 121-131 (1979).

[6] L. G. Sillen, "X-ray studies on bismuth trioxide," *Ark. Kemi. Mineral Geol.***12A**, 1-15 (1937).

[7] E. M. Levin and R. S. Roth, *J. Res. Natl. Bur. Std.* **68A**, 197 (1964).

[8] G. M. Saffronov, V. N. Batog, T. V. Stepanyuk and P. M. Federov, *Russ. J. Inorg. Chem. (Engl. Transl.)* 16, 460 (1971).

[9] T. M. Bruton, O. F. Hill, P. A. C. Whiffin and J. C. Brice, *J. Cryst. Growth* **32**, 27 (1976).

[10] D. C. Craig and N. C. Stephenson, *J. Solid State Chem.* **15**, 1 (1975).

[11] S. F. Radaev and V.I. Simonov, *Kristallografiya* **37**, 914 (1992).

[12] A. V. Kosov, V. A. Kutvitskii, V. M. Skorikov, O. N. Ustalova and T. I. Koryagina, "Phase-diagram of system Bi_2O_3-ZnO," *Inorganic Materials* **12**, 401-404 (1976).

[13] J. P. Guha, Š. Kunej and D. Suvorov, "Phase equilibrium relations in the binary system Bi_2O_3-ZnO," *J. Mater. Sci.* **39**, 911-918 (2004).

[14] D. R. Clarke, "Grain-boundary segregation in a commercial ZnO-based varistor," *J. Appl. Phys.* **50**, 6829-6832 (1979).

[15] E. P. Rothman, "Activated sintering of bismuth-doped zinc oxide ceramics," Master's Thesis, MIT, Cambridge, Massachusetts, 1982.

[16] J.-H. Hwang, T. O. Mason, and V. P. Dravid, "Microanalytical determination of ZnO solidus and liquidus boundaries in the ZnO-Bi_2O_3, System," *J. Am. Ceram. Soc.* **77** 1409-1504 (1994).

[17] T. Takemura, M. Kobayashi, Y. Takada and K. Sato, "Effects of bismuth sesquioxide on the characteristics of ZnO varistors," *J. Am. Ceram. Soc.* **69**, 430-436 (1986).

[18] H. Cerva and W. Russwurm, "Microstructure and crystal structure of bismuth oxide phases in zinc oxide varistor ceramics," *J. Am. Ceram. Soc.*, **71,** 522-30 (1988).

[19] E. D. Kim, M. H. Oh, C. H. Kim, "Effects of annealing on the grain boundary potential barrier of ZnO varistor," *J. Mater. Sci.* **21**, 3491-3496 (1986).

[20] E. Olsson, G. Dunlop and R. Österlund, "Development of functional microstructure during sintering of a ZnO varistor material," *J. Am. Ceram. Soc.* **76**, 65-74 (1993).

[21] E. Olsson, G. L. Dunlop and R. Österlund, "Development of interfacial microstructure during cooling of a ZnO varistor material," *J. Appl. Phys.* **66**, 5072-5077 (1989).

[22] M. Inada, "Effects of heat treatment on crystal phases, microstructure and electrical properties of nonohmic zinc oxide ceramics," *Jpn. J. Appl. Phys*. **18**, 1439-1446 (1979).

[23] A. Iga, M. Matsuoka and T. Masuyama, "Effect of phase transition of intergranular Bi_2O_3 layer in nonohmic ZnO ceramics," *Jpn. J. Appl. Phys*. **15**, 1161-1162 (1976).

[24] M. N. Rahaman, L.C. De Jonghe, J.A. Voigt and B.A. Tuttle, "Low-temperature sintering of zinc oxide varistors," *J. Mater. Sci.* **25,** 737-742 (1990).

[25] W. F. Hammetter and J. A. Voigt, "Effect of Na on the phase relationships at the Bi-rich end of the ZnO-Bi_2O_3 phase diagram," Pres. at 93rd Annual Mtg. of the Am. Ceram. Soc., Cincinnati, OH, April 28 – May 2, 1991.

[26] J. Kim, T. Kimura and T. Yamaguchi, "Effect of bismuth oxide content on the sintering of zinc oxide," *J. Am. Ceram. Soc.* **72** 1541-1544 (1989).

[27] T. J. Gardner, W. F. Hammetter and B. A. Tuttle, "Microstructure/property relations in the sintering of chemically prepared varistor materials," pres. at the Annual Meeting of the Am. Ceram. Soc., 1985.

[28] K. S. Kirkpatrick, T. O. Mason, U. Balachandran and R. B. Poeppel, "Impedance spectroscopy study of sintering in Bi-doped ZnO**,"** *J. Am. Ceram. Soc.* **77**, 1493-1498 (1994).

[29] T. J. Gardner and W. F. Hammetter, "Densification kinetics of high field varistor materials," pres. at the Annual Meeting of the Am. Ceram. Soc., 1986.

[30] T. J. Garino, B. A. Tuttle, M. S. Harrington and J. L. Yio, "Sintering studies on high field varistors," Sandia National Laboratories Report SAND89-0782, 1989.

[31] J. Luo, H. Wang and Y.-M. Chiang, "Origin of solid state activated sintering in Bi_2O_3-doped ZnO," *J. Am. Ceram. Soc.* **82** 916-920 (1999).

[32] T.J. Gardner and S.J. Lockwood, "Sintering schedule and sample geometry effects on the electrical and physical properties of high field varistor materials," Sandia National Laboratories Report SAND88-2449, 1989.

[33] S. J. Lockwood, "Restart of the chemical preparation process for the fabrication of ZnO varistors for ferroelectric neutron generator power supplies," Sandia National Laboratories Report SAND2005-0763U, March 2005.

[34] S. J. Lockwood, private communication, 2005.

[35] M. Peiteado, M.A. de la Rubia, M.J. Velasco, F.J. Valle and A.C. Caballero, "Bi_2O_3 vaporization form ZnO-based varistors," *J. Euro. Ceram. Soc.* **25**, 1675-1680 (2005).

[36] M. A. de la Rubia, M. Peiteado, J. F. Fernandez and A. C. Caballero, "Compact shape as a relevant parameter for sintering ZnO– Bi_2O_3 based varistors," *J. Euro. Ceram. Soc.* **24**, 1209-1212 (2004).

[37] M. Matsuoka, "Nonohmic properties of zinc oxide ceramics," *Jpn. J. Appl. Phys*. **10**, 736-746 (1971).

[38] W. D. Kingery, J. B. Vander Sande and T. Mitamura, "A scanning transmission electron microscopy investigation of grain-boundary segregation in a ZnO- Bi_2O_3 varistor," *J. Am. Ceram. Soc.* **62**, 221-22 (1979).

[39] D. R. Clarke, "The microstructural location of the intergranular metaloxide phase in a zinc oxide varistor," *J. Appl. Phys.* **49**, 2407-11 (1978).

[40] M. Inada, "Microstructure of nonohmic zinc oxide ceramics," *Jpn. J. Appl. Phys*. **17**, 673-77 (1978).

[41] W. G. Morris, "Physical properties of the electrical barriers in varistors," *J. Vac. Sci. Technol.* **13**, 926-31 (1976).

[42] H. Kanai, M. Imai and T. Takahashi, "A high-resilution transmission electron microscope study of a zinc oxide varistor," *J. Mater. Sci*. **20**, 3957-66 (1985).

[43] K.-I. Kobayashi, O. Wada, M. Kobayashi and Y. Takada, "Continuous existence of bismuth at grain boundaries of zinc oxide varistor without intergranular phase," *J. Am. Ceram. Soc.* **81**, 2071-2076 (1998).

[44] E. Olsson and G.L. Dunlop, "Characterization of individual interfacial barriers in a ZnO varistor material," *J. Appl. Phys.* **66**, 3666-3675 (1989).

[45] H. Wang and Y.-M. Chiang, "Thermodynamic stability of intergranular amorphous films in bismuth-doped zinc oxide," *J. Am. Ceram. Soc.* **81**, 89-96 (1998).

[46] J. P. Gambino, W. D. Kingery, G. E. Pike, L. M. Levinson and H. R. Philipp, "Effect of heat treatments on the bismuth-rich intergranular phases in ZnO:Bi:Co varistors," *J. Am. Ceram. Soc.* **72**, 642-645 (1989).

[47] I. Baumgartner and R. Einzinger; pp. 367-371 in Sintering – Theory and Practice. Ed. By D. Kolar, S. Pejovnik and M. M. Ristic. Elsevier Scientific Pub. Co., Amsterdam, Netherlands, 1982.

[48] J.-G. Li, "Some observations on wetting in the Bi_2O_3-ZnO system," *J. Mater. Sci. Let.* **13**, 400-403 (1994).

[49] F. Stucki and F. Greuter, "Key role of oxygen at zinc oxide varistor grain boundaries," *Appl. Phys. Lett.* **57**, 446-448 (1990).

[50] P. R. Bueno, E. R. Leite, M. M. Oliveira, M. O. Orlandi and E. Longo, "Role of oxygen at the grain boundary of metal oxide varistors: A potential barrier formation mechanism," *Appl. Phys. Lett.* **79**, 48-50 (2001).

[51] E. Sonder, M. M. Austin and D. L. Kinser, "Effect of oxidizing and reducing atmospheres at elevated temperatures on the electrical properties of zinc oxide varistors," *J. Appl. Phys.* **54**, 3566-72 (1983).

[52] M. A. Ramírez, A. Z. Simões, P. R. Bueno, M. A. Márquez, O. Orlandi and J. A. Varela, "Importance of oxygen atmosphere to recover the ZnO-based varistors properties," *J. Mater. Sci.* **41**, 6221–6227 (2006).

[53] E. M. Levin and R. S. Roth, "Polymorphism of bismuth sesquioxide. I.", *J. Res. Natl. Bur. Std.* **68A**, 189-195 (1964).

Distribution

1	0885	Gordon Pike, 01820
1	1245	Steve Lockwood, 02454
1	1245	Alex Roesler, 02454
1	1245	Chris Diantonio, 2454
1	1349	Bill Hammetter, 01815
1	1349	Tom Hinklin, 01815
1	1411	Terry Garino, 01816
1	1411	Mark Rodriguez, 01812
1	1411	Jim Voigt, 01816
1	1411	Bruce Tuttle, 01816
1	9018	Cental Technical Files, 8945-1(electronic copy)
1	0899	Technical Library, 09616 (electronic copy)


Sandia National Laboratories